From the Clinics for Pediatrics II

(Acting director: PD. Dr. Andreas van Baalen)

at the University Medical Center Schleswig-Holstein (UKSH), Campus Kiel
at Kiel University

Neuronal networks underlying Jeavons-syndrome and eye closure sensitivity by using EEG source analysis methods

Dissertation to

acquire the doctoral degree (Dr. med.)

at the Faculty of Medicine

at Kiel University

presented by

MARIAM ABULADZE

from Georgia

Kiel (**2021**)

1st Reviewer: Prof. Dr. Ulrich Stephani, Klinik für Kinder- und Jugendmedizin II

2nd Reviewer: Priv. -Doz. Dr. Nils Gerd Margraf, Klinik für Neurologie

Date of oral examination: 15.12.2022

Approved for printing, Kiel 24.08.2022

Signed: Prof. Dr. Franziska Theilig

Content

Acknowledgement

First and foremost, I am extremely grateful to my PhD supervisor, Prof. Dr. Ulrich Stephani, for his invaluable advice, continuous support, encouragement and patience during my doctoral studies.

I would also like to thank Dr. N. Japaridze for her great support and supervision. Her immense knowledge and rich experience encouraged me during my academic research.

My special thanks goes to Prof. Nana Tatishvili, who has been my mentor for the past years.

I would also like to thank Ms. Lyschko and Dr. Hamid for conducting the eLORETA and iCOH connectivity analysis and for their valuable contribution for the progression of this research work.

I would like to thank Dr. Ami Kumar for her friendship and support during my/our PhD research.

I would like to thank the DAAD and the International Center of CAU for their financial support.

My special thanks go to the wonderful women from the International Café at CAU, who have managed and hopefully will continue to manage to help international students get to know Kiel and the university.

Finally, thank you Kiel, we have experienced many new things together.

1. Introduction

1.1 Historical background

The first report about eyelid myoclonia comes from 1932: Radovici and colleagues described a clinical case of a 20 years old man, who from the childhood age had photically induced "frequent and spasmodic blinking of the eyelids with rhythmical movements of both rotating and elevating of the head towards the sun" (Radovici et al., 1932).

Eyelid myoclonia with absences (EMA), or Jeavons syndrome (JS), was first described by Jeavons: "Eyelid myoclonia and absences show a marked jerking of the eyelids immediately after eye closure and there is an associated brief bilateral spike and wave activity. Brief absences may occur spontaneously, accompanied by 3/sec spike-waves. The spike-waves after eye closure do not occur in the dark. Their presence in the EEG is a reliable warning that abnormalities will be evoked by photic stimulation" (Jeavons, 1977).

Later in 1996 Duncan and Panayiotopoulos wrote a book about this syndrome, "Eyelid myoclonia with absences", where they suggested to name this condition as Jeavons Syndrome (JS).

According to the 2006 International League Against Epilepsy (ILAE) classification of epileptic syndromes, JS was not recognized as an epileptic syndrome (Engel, 2006). However, eyelid myoclonia was classified as a reflex idiopathic generalized epilepsy (IGE) by Panayiotopoulos (2005a) because of the presence of normal posterior dominant background activity, paroxysmal generalized ictal EEG discharges, and photosensitivity (Panayiotopoulos, 2005a).

The latest ILAE position paper of the operational classification of seizure types proposes that "absence with eyelid myoclonia" is a "new nonmotor seizure type" (Fisher et al., 2017a; Fisher et al., 2017b).

1.2 Demographic Data

The prevalence of JS is around 13% of all idiopathic generalised epilepsies. Relation of occurrence in girls is twice that in boys (Panayiotopoulos, 2010).

1.3 Clinical manifestation

Jeavons syndrome is age-dependent, onset typically in childhood with a peak at age 6-8 years (range 2-14 years).

1.3.1 Seizure type

The clinical event of Jeavons syndrome consists of repetitive, rhythmic, fast myoclonic jerks of the eyelids, which can be followed with the impairment of consciousness - absences. During the absence, the eyelid jerking becomes less violent than in the onset. Impairment of consciousness is not severe and manifests with cessation, repetition, errors and delays of counting on video-EEG (Duncan et al., 1996). Seizures are brief, lasting 3-5 seconds; usually multiple per day and are provoked by eye closure. It is quite different from other eyelid movements. Often eyelid jerks are accompanied with vertical jerking and upward deviation of the eyeballs, together with jerks of the eyebrows and the head. In addition, the lateral deviation of the eyes and the head can appear. Eyelid myoclonia may also be associated with jerks of the hands. An eyelid myoclonic status epilepticus is reported in up to twenty percent of the patients. (Panayiotopoulos, 2010).

In the majority of the patients rare generalized tonic-clonic seizures (GTCS) may occur, which are often precipitated or facilitated by sleep deprivation, alcohol abuse, poor drug compliance, flickering light, television or video-game exposure (Panayiotopoulos, 2005).

The most provocative factor for eyelid myoclonia is eye closure in the presence of uninterrupted light (eye closure sensitivity). Eye closure in total darkness is ineffective. Photosensitivity declines with age, whereas eye closure remains a lifelong precipitating factor (Giannakomidos and Panayiotopoulos, 1996).

1.3.2 Electroenephalography (EEG)

Interictal EEG mostly shows high amplitude discharges of spike and slow waves at 3-6 Hz. (Caraballo et al., 2009). They are brief (1-5 seconds) and often appear immediately (within 0.5-2 seconds) after closing the eyes (eye closure sensitivity, ECS) in an illuminated room (Duncan and Panayiotopoulos., 1996) Photoparoxysmal responses are present in all untreated patients but may be absent in older patients on medication. EEG discharges are also pronounced by hyperventilation.

Ictal EEG during eyelid myoclonia are generalised discharges of mainly polyspikes and polyspike-slow waves with frequency 4 to 6 Hz. The very common precipitating factor for eyelid myoclonia and EEG aggravation is awakening (Caraballo et al., 2009).

1.4 Pathogenesis and etiology

1.4.1 Pathogenesis

The underlying pathogenesis of EMA is poorly understood. It is presumed, that there is a malfunction of alpha rhythm generators in the occipital lobe (Panayiotopoulos, 2010) and that both magnocellular and parvocellular systems of the lateral geniculate nucleus of the thalamus are functionally disturbed (Wilkins, 1999).

According to clinical and neuroimaging studies, the occipital visual cortex plays a main role in the generation of EMA in the presence of light and eye closure (Viravan et al., 2011). Some consider that activation of brainstem structures are also involved in the epileptic neuronal network of EMA (Vaundano et al., 2014).

Previous clinical studies (Viravan et al., 2012; Mourente-Diaz et al., 2007; Ogura et al., 2005) revealed a high incidence of focal interictal epileptiform discharges (EDs) from the posterior brain regions, and some focal posterior ictal epileptiform discharges preceding generalized epileptiform discharges. The EEG study of Viravan in 12 children with JS, showed that 11 patients (92%) had focal posterior ictal EDs. All focal ictal EDs were described as either posterior EDs, occurring 200 ms to 1 s before generalized EDs (9 patients), or posterior EDs alone (2 patients) predominantly over the occipital region. Spiky posterior alpha activities appeared at eye closure and during sustained eye closure in half of the children with JS. These spiky posterior alpha activities in JS may support the hypothesis of alpha rhythm generator malfunction in the occipital lobe (Viravan et al., 2011).

Mourente-Diaz described unusual focal ictal EEG finding in two patients with EMA and mild developmental delay. Both of them had a normal background activity. Bilateral occipital polyspikes or spike-wave complexes were described during EMA immediately after eye closure in both patients (Mourente-Diaz., 2007).

Ogura and colleagues also described a 14-year-old girl with EMA. Ictally, generalized spike and wave discharges were always preceded by paroxysmal beta burst activity in the occipital region, giving the presumption that the elimination of fixation on visual cues in the light could trigger the occipital spikes (Ogura et al., 2005).

Liu conducted a study to investigate the blood oxygenation level-dependent (BOLD) signal

changes correlated with ictal and interictal epileptic discharges using electroencephalography-correlated functional magnetic resonance imaging (EEG-fMRI) in patients with eyelid myoclonia with absences (EMA). Four patients with EMA were investigated through the method of EEG-fMRI. The characteristics of BOLD signal changes linked to ictal and interictal epileptic discharges under different states of consciousness were explored. The main regions of activation included thalamus, mesial frontal cortex, middle parietal lobe, temporal lobe, insula, midline structures, and cerebellum. Deactivations were mainly in the anterior frontal lobe, posterior-parietal lobe, and posterior cingulate gyrus. The thalamic BOLD change was predominantly activation in most of the cases. The distribution of activation associated with ictal epileptic discharges was wider than during interictal epileptic discharges (Liu et al., 2008). Vaudano investigated the functional and structural brain changes associated with eyelid myoclonus and absence seizures triggered by eye closure (ECS). 13 EMA patients, 14 patients with idiopathic generalized epilepsies (IGE) with ECS, and 16 healthy controls (HC) underwent EEG-fMRI and voxel-based brain morphometry (VBM) protocol. In EMA patients compared to HC and IGE, they found: (1) higher blood oxygenation level-dependent (BOLD) signal related to the eye closure over the visual cortex, the posterior thalamus, and the network implicated in the motor control of eye closure, saccades, and eye pursuit movements; and (2) increments in the grey matter concentration at the visual cortex and thalamic pulvinar, whereas decrements were observed at the bilateral frontal eye field area (Vaudano et al., 2014).

1.4.2 Etiology

The etiology of Jeavons syndrome is unknown. According to a broad genetic study of idiopathic generalized epilepsies, the cases of eyelid myoclonia with absences in the family members of probands were found (Bianchi, 1995), which suggest its genetical determination.

Parker and colleagues reported that of 18 patients with eyelid myoclonia with absences, 14 had family history of epilepsy (Parker et al., 1996). Four patients had other family members affected by a similar type of epileptic condition. Eyelid myoclonia with absences has been reported in monozygotic twins (Adachi et al., 2005). It has also been described the evolvement of benign myoclonic epilepsy of infancy (Moutaouakil et al., 2010) or cryptogenic myoclonic epilepsy of early childhood (Ohya et al., 2012) in EMA.

In a study, by Sadleir and colleagues (2012), family members of individuals with eyelid myoclonia with absences were assessed for seizures. 18 individuals with eyelid myoclonia with

absences were recruited. A history of seizures was found in 34 relatives in 15 (83%) of 18 families.

Several gene mutations have been associated with eyelid myoclonia with or without absences, which is confirmed through the different reports and studies. Rudolf et al conducted whole-exome sequencing in a family with the diagnosis of eyelid myoclonia with absences. They found a nonsense variant (c.196C4T/p.(Arg66*)) in RORB, which encodes the beta retinoid-related orphan nuclear receptor (RORβ), in four affected family members (Rudolf et al., 2016). Galizia tried to determine whether CDH2 gene variations underly photosensitivity in common epilepsies, specific photosensitive epilepsies and individuals with photosensitivity but without seizures. They studied 580 individuals with epilepsy and either photosensitive seizures or abnormal photoparoxysmal response on electroencephalography, or both, and 55 individuals with photoparoxysmal response but no seizures. Among epilepsy syndromes, they found over-representation of unique CHD2 variants (3/36 cases) in the archetypal photosensitive epilepsy syndrome, eyelid myoclonia with absences (Galizia et al., 2015).

Samanta and colleages reported one case of Jeavons syndrome in a female patient with a pathogenic de novo frameshift mutation of KIAA2022 with four nucleotides missing at position 1718_1721. This gene has been already identified in 13 female patients with intellectual disability and epilepsy (Samanta et al., 2018).

Marini et al describe the electroclinical features and long-term follow-up of 6 novel patients carrying de novo missense and nonsense KCNB1 mutations. The phenotype was wide-ranging from Lennox-Gastaut syndrome to remitting infantile spasms and to mild generalized epilepsy. Among them was one female patient with eyelid myoclonia with absences (Marini et al., 2017).

1.5 Management

The treatment approach is the same as for the idiopathic generalized epilepsies. Sodium valproate and ethosuximide combination are considered the most effective for treating patients with EMA. Levetiracetam, as an antimyoclonic drug, is also often a successful treatment option. In most cases of JS, a polytherapy is necessary and a many cases stay drug-resistant (Panayiotopoulos, 2010; Panayiotopoulos, 2005; Striano et al., 2009).

1.6 Prognosis

Mostly EMA is difficult to treat. Frequent eyelid myoclonia, usually without absences stay lifelong. The neurophysiologic functioning of JS has not been well described yet, despite the suggestion that a subtype of the syndrome is characterised by cognitive impairment. Capovilla

et al. conducted a retrospective study of 18 patients with EMA. All patients had a long follow-up, more than 10 years in the large majority of subjects (16 of 18) and more than 15 years in 10 of 18 patients. All the patients showed varying degrees of impaired intellectual functioning. Besides, the patients showed behavioural disturbances with hyperkinetic features. In four patients, EM disappeared during or after adolescence. In 11 patients, EM remained unchanged or reduced only slightly. Tonic-clonic seizures decreased in their frequency after the third decade of life but completely disappeared in only five patients (Capovilla et al., 2009).

In one study Fournier-Goodnight and colleagues tried to define neurocognitive functioning in pediatric patients with JS, by examining global IQ and relevant neurocognitive domains. Statistical analyses revealed performance that was below average on measures of global IQ, ranging from low average to borderline impaired (Fournier-Goodnight et al., 2015).

Arivo et al described a clinical outcome of 4 women with JS using Wechsler test. Three out of four EMA patients turned out to be intellectually disabled. By these patients, the right diagnoses were delayed and narrow-spectrum antiepileptic drugs were prescribed, where´s the fourth patient with the best cognition had been treated with broad-spectrum anticonvulsants, recommended for EMA. The author finds some connection between appropriate treatment and neurocognitive outcome (Arivo et al., 2018).

1.7 Functional connectivity analyses

EEG is a most useful laboratory tool to diagnose epilepsy and to classify seizure types or epilepsy syndromes. It has many benefits: it is non-invasive, has an excellent temporal resolution, is less prone to movement artefacts and less expensive compared to other high technology diagnostic tools, and it may be recorded for a longer period.

Nevertheless, EEG signals measured on the scalp surface do not give precise information about the location of the active neurons in the brain due to some underlying static electromagnetic inverse problem. Especially it is most challenging to measure electric sources in deep brain structures (Holmes, 2009; Holmes et al., 2004). However, recent development in EEG source analyses, and advancements in inverse and forward solutions allows us to improve the temporal resolution of the scalp EEG recordings and gives a better interpretation of different parts of neuronal networks (Groening et al., 2009; Siniatchkin et al., 2010; Vulliemoz et al., 2011). During the assessment of normal EEG, detecting and differentiating the ictal and interictal EEG activity is based on visual inspection, which is not completely reliable. Subtle changes during

ictal and interictal EEG discharges remain undetectable, because they are impossible to capture with pure visual examination (Tharp et al., 1975).

Epilepsy itself is a network disorder, which means that functional and effective connectivity of the brain is impaired. The term functional connectivity refers to a functionally integrated relationship (functional coupling) between spatially separated brain regions. Recently, a considerable literature has grown up around the theme of functional connectivity during several brain disorders. Among them are the studies on epilepsies with focusing on understanding the pathological network disorders following the seizure onset. Several attempts have been made to quantify the spatio-temporal functional connectivity of different brain segments to reveal their dynamic behavior. One of them is quantitative EEG analysis, which means applying various algorithms on EEG data and transforming them in the time-frequency domain. It is known that functionally connected neurons tend to fire synchronously and exactly the frequency of synchronization seems to define the functional state of connectivity, whether it is normal or abnormal (Kropotov, 2009).

The measure for functional connectivity is coherence, which means the measure of synchronization between EEG signals, recorded in different scalp locations. It reflects a correlation between EEG powers computed for these two locations in the same frequency band (Kropotov, 2009).

To analyze the FC, it is possible on both the sensor (scalp) and source level.

In contrast to source level FC, sensor level FC analysis directly uses scalp surface EEG signals. It has already been used for assessing epilepsy (Brazier, 1972; Gotman, 1981; Song et al., 2013) and other brain disorders like schizophrenia (Shim et al., 2016) or anesthesia states assessment (Dressler et al., 2004). The signal processing method called power spectral analysis gives the possibility to perform sensor level EEG connectivity analysis and allows to get the frequency maps of power parameters. Such kind of voltage maps allows estimating of the location and orientation of the source (Kane et al., 2017). The frequency-based technic such FFT has already been used by several researchers to analyse the EEG spectral pattern (Meenakshi et al., 2014, Thieu et al., 2015).

To investigate the functional connectivity on the source level and understand the involvement of deeper structures of the brain in the epileptic network, so-called inverse and forward problems must be solved. The main attempt in source level functional connectivity analysis is the source localization. Applying signal processing techniques on the measurements of the EEG potentials from the different electrodes gives the estimation of current sources inside the brain. Generally, the neuronal activity can be modelled as an electrical currents dipole (Michel, 2012).

The source localization is divided into two main steps. First finding the scalp potentials which could probably come out from the hypothetical dipoles or in other words, from a current distribution inside the head. This step is called Forward problem solution. The second step is using the data measured from certain electrodes on the scalp to work back and estimate the sources that best fit this data, the so-called inverse problem solution (Grech et al., 2008).

The forward problem solution starts with reconstruction modelling of lead field matrix (LFM), which determines how the electrical activity at a certain electrode is related to the activity of the different sources in the brain (Michel, 2009). The exact low-resolution brain electromagnetic tomography (eLORETA) is a good solution to the inverse problem, which gives an opportunity of exact localization and computation of the cortical 3D distribution of current density (Pascual-Marqui, 2011).

For the FC analysis, the coherence method is used to understand how the given sources are interrelated. Nolte proposed and demonstrated the usage of the imaginary part of coherency (iCOH) for identifying true brain interaction from EEG data on the simple motor task example (Nolte et al., 2004). Later iCOH was used successfully to analyse the FC in the children with ASD (García Dominquez et al., 2013).

1.8 Aims of the study

On the sensor level, the study aimed to investigate frequency-dependent neuronal oscillations underlying EMA, eye closure sensitivity. We tried to answer the question whether significant differences of frequency power exist between ictal and interictal discharges after eye closure using spectral analysis.

On the source level, we tried to localize the source maximum using eLORETA and investigated Functional connectivity (FC) based on imaginary part of coherency (iCoh), to find out, if there are different neuronal networks involved during ictal (myoclonic seizure) and interictal EEG discharges in EMA Patients after eye closure.

In summary, the main question of the study was, if the spikes and waves in the EEG ictally and interictally can be discriminated by using sensor and source level EEG analyses.

2. Materials and Methods description

2.1 Materials

2.1.1 Subjects

The data (EEG, clinical information) of 16 Patients from Northern German epilepsy center for children and adolescents with the diagnosis of Jeavons syndrome were retrospectively and prospectively collected and analysed. 5 patients were excluded because of the lack of appropriate ictal and interictal EEG segment. All 200 EEG recordings of the 11 patient (8 female/3male) from the year 2006 to 2018 were selected.

The study was conducted according to the Declaration of Helsinki (current version, 2013) on biomedical research involving human subjects (Tokyo amendment, AZ.: D 456/19).

Table 1. Demographic and clinical data

Patient (Gender)	**Family history**	**Diagnosis**	**Development**	**Seizure onset**	**Seizure type**	**Medication**	**Brain imaging**	**Photosensitivity, grade**
1 (m)	No	JS	Good	4 y	EM	LEV, ETH, VPA	Normal	IV
2 (f)	No	JS	Good	6 y	EM	VPA, LMG	Normal	—
3 (f)	No	JS	Mild delay	3 Y	EM, Abs	VPA, ZNS, TPM, LMG	Normal	IV
4 (f)	No	JS	Good	7 y	Abs, EM	STM, VPA, LMG, ETH, LEV, TPM	Normal	_
5 (m)	No	JS	Mild delay	3 y	EM , Abs, GTCS	VPA, ETH ,LMG, LEV, TPM, ZNS	Normal	IV

6 (m)	No	JS	Good	6 y	EM Abs,	LMG, VPA, ESM	Normal	IV
7 (f)	FS-aunt	JS	Mild delay	8y	Abs, EM, GTCS	ESM, VPA LEV	Normal	IV
8 (f)	FS Brother	JS	Mild delay	4y	EM Abs, GTCS	LMG, VPA, LEV, ETH	Normal	IV
9 (f)	No	JS	Good	7 y	GTCS, EM, Abs.	SLT. VPA, LEV ,LMG ,ETH	Normal	IV
10 (f)	No	JS	Good	6 y	EM, Abs, GTCS	ETH, VPA LMG, LEV	Normal	
11 (f)	No	JS	Mild delay	5 y	EM, LM, MS	LMG, VPA, VNS, ETH, LEV, TPM	Gen. Atrop hy	IV

JS –Jeavons syndrome; EM-eyelid myoclonus; GTCS – generalised tonic-clonic seizures; Abs-absences; FS-febrile seizures; LM –Limb Myoclonus; MS-Myoclonic Status. VPA – Valproic Acid; LEV – Levetiracetam; STM – sulthiame; TPM – Topiramate; VNS- Vagus Nerves Stimulation; LTG
– Lamotrigine; ETH-Ethosuximide. Photosensitivity grade according (Waltz et al., 1992).

All patients had eyelid myoclonia as the main seizure type. Development before seizure onset in all cases was normal. Mean age of seizure onset was 5, 4 years. (Median 6, SD=1, 6). All of them were receiving several AED (antiepileptic drugs) during the clinical course. Photo paroxysmal response grade IV was observed in most of the patients.

2.1.2 EEG recordings

Standard EEG recordings, according to the 10/20 system (EEG recording system: Neurofile;

IT-med, Bad Homburg, Germany) taken during the routine admissions in the epilepsy center were used for the analyses. Sintered Ag/AgCl ring electrodes with built-in 5 kOhms resistors were attached using the “EasyCap” (Falk-Minow Services, Herrsching-Breitbrunn, Germany). Impedance was kept below 10 kΩ, the sampling rate was 512 Hz. Reference was located between Fz and Cz.

All the patients had generalised spikes/polyspike and wave discharges. Eye closure sensitivity was defined as ictal or interictal discharge occurring less than 4 seconds after eye closure. The ictal event was only eyelid myoclonia. Segments with absences and limb myoclonus were not included.

2.1.3 Selection of epochs

The visual inspection of EEGs, segments selection and marking was performed with BESA (www.BESA.de) research 7.0 software. Following segments of interest were selected: Segments of the ictal EEG discharges with eyelid myoclonia (triggered by eye closure) (Figure 1.) and EEG segments with eye closure induced interictal EEG discharges without clinical manifestations (Figure 2.). The minimal duration of discharge was 1 sec. The discharges less than 1 second were not included.

To analyse network changes after eye closure, selected epochs were divided into two parts: a. - segments 3 seconds before discharge -preictal / preinterictal and b. segments of discharge – during ictal / during interictal and were analysed separately.

Paroxysmal discharges and eyelid myoclonia induced during photic stimulation, hyperventilation and sleep were excluded.

Figure 1. EEG recording showing eyelid myoclonia appearing soon after eye closure

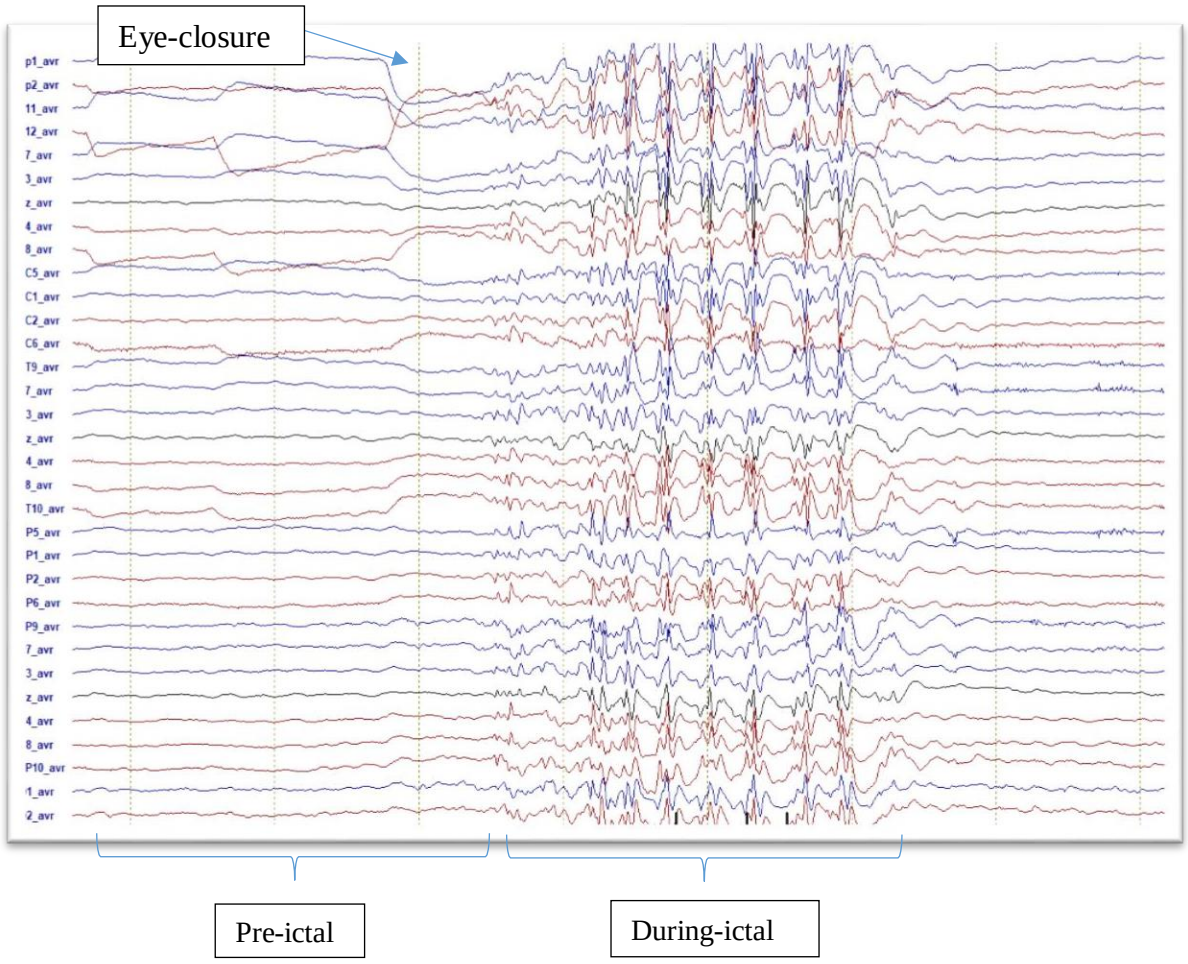

Figure 2. EEG recording showing interictal discharge appearing soon after eye closure

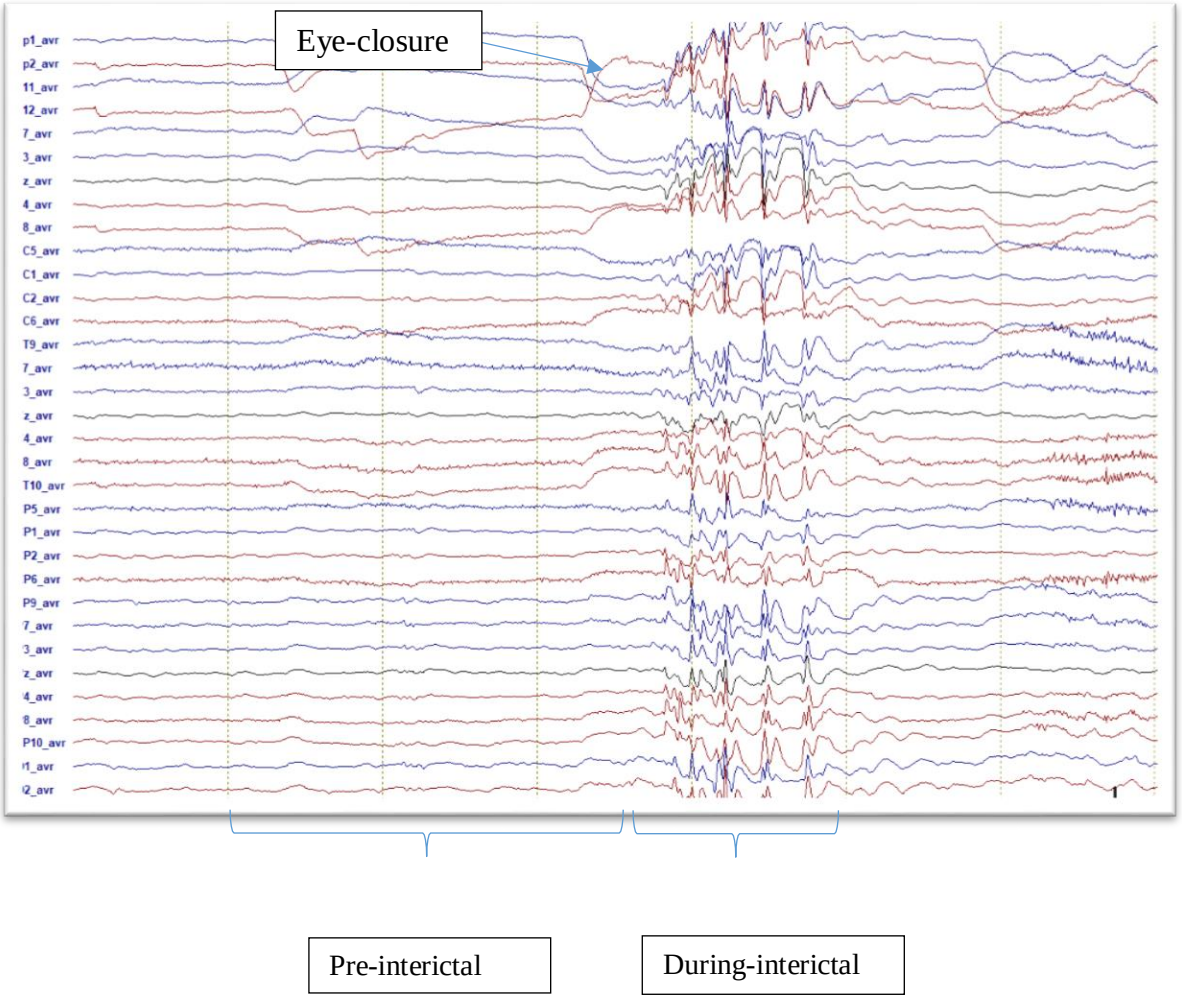

2.2 Methods

2.2.1 Sensor level analysis

As already mentioned in chapter 1 the signal processing method called power spectral analysis gives the possibility to perform sensor level EEG connectivity analysis. The power spectrum reflects the frequency content of the distribution of signal power over frequency (Dressler et al., 2004). The EEG spectral analysis quantifies the amount of rhythmic, oscillatory activity of different frequencies in EEG which are not detectable with a visual inspection. Spectra is computed utilizing Fourier transform, that decomposes EEG signals into a series of sinusoidal functions with different frequencies, amplitude and phases (Kropotov, 2009). The Fourier transform is based on Fourier theorem, which confirms that any waveform can be decomposed into a sum of sine waves at different frequencies (Kim et al., 2011). After getting the frequency maps of the power of the EEG potentials the location of the source accordingly to the power maximum can be localised.

2.2.2 Source level analysis

As already described in the introduction in order to find the source of the epileptic activity in the brain two problems, so-called inverse and forward problem has to be solved.

The forward problem solution starts with the reconstruction of lead field matrix (LFM), which itself represents the mapping between the brain dipoles and electrodes and computes the scalp potential differences from the source activity (Koenig, 2014).

Constructing the forward model is the specification of ellipsoidal head models of head conductivity with finite different computations (Salman et al., 2005).The head models are based on biologically realistic assumptions such as the geometry and the electrical properties of the head tissues (Nunez et al., 1997). The volume conduction models show how the currents flow through the tissue but it does not include the information about the origination of the signal. The main property of the head model is the description of the head geometry. There are several head model options, from simple sphere to realistic head models. One of them is MNI (Montreal Neurological Institute) head model which is 3 Layer template of BEM (Standard Boundary Element Method) model. The BEM model is based on the segmentation from the anatomical model of normal Brain and is expressed in MNI coordinates in mm (Oostenveld et al., 2003). Here the dipole localization is visualized in relation to a standard brain MRI model, with

electrodes positioned in relation to the scalp landmarks and coregistered with the head conductivity model (Holmes et al., 2004).

The main challenge in the inverse problem solution is that for the given scalp potentials, there can be found an endless number of dipoles that would produce given EEG signals. The task, in this case, is to use additional tools to select among these infinite number of valid inverse solutions.

The novel Method the exact low-resolution brain electromagnetic tomography (eLORETA), solves the inverse problem and gives an exact localization and computation of the cortical 3D distribution of current density (Pascual-Marqui, 2007). It is a discrete, 3D distributed, linear weighted minimum norm inverse solution, and presents an improved version of previous tomography versions, like LORETA (Pascual-Marqui, 1994) and sLORETA (Pascual-Marqui, 2002), as it has no localization bias even in the presence of structural noise. Additionally to this eLORETA can localize deep structures of the brain correctly.

eLORETA has already been successfully used to localize function in the primary and secondary sensory cortices (Pascual-Marqui, 2002). Several groups have used eLORETA for resting-state source localisation and FC (Aoki et al., 2015), (Canuet et al., 2011). Adebimpe et al was first who used eLORETA to analyze cortical sources in patients with epilepsy (Adebimpe et al., 2016).

2.2.3 Connectivity analysis using Imaginary part of Coherency (iCoh)

Solving the inverse problem gives us information which brain regions are involved in the generation of certain waves, but it does not present how these brain regions are interrelated and how these source activities functionally connected are.

To solve this problem the coherence method must be used, which provides a measure of linear similarity between signals in the frequency domain. Functional connectivity analysis in the frequency domain based on the coherence method has been widely proposed (Fries, 2005; Nunez et al., 1997; Gross et al., 2005).

Coherency between EEG channels is interpreted as a reflection of the interaction between different brain areas. The activity of a single source can be measured in many EEG channels which gives the main challenge and is referred to as Volume conduction (VC). Exactly this strong volume conductivity effect makes the proses of FC analyses difficult (Nolte et al., 2004). Nolte proposed improved coherence method called Imaginary part of Coherency (iCoh) to avoid the VC effect for the estimation of FC. The main idea of this method is, to avoid artefact

of VC, by trying not to interpret it as a brain interaction. This method is based on the assumption that the observed scalp potential has no time lag to the underlying source activity (Nolte et al., 2004). iCoh cancels out all sources of external coherence that are the result of the prompt activity of artifactual results caused by volume conduction. What is left, the imaginary part, captures true source interaction at a given time lag (Nolte et al.,2004).

3. Steps of analysis

3.1 Sensor-level analysis

3.1.1 Preprocessing

The EEG data was bandpass filtered in the range between 0.1 Hz and 31 Hz. Then Independent component analysis (ICA) was used to remove eye- blink and eye-movement artefacts. ICA is a statistical method to transform the data in such a linear way that the results can become statistically independent. It cancels the addictive background noise and separates the mixed signals (Choi, 2012).

After these, the EEG channels were re-referenced to the common average reference (CAR) For selected segment z-score transformation was performed for every subject. Pre-selected EEG intervals were divided into 1-second-long segments and the mean and the trend were removed for them.

3.1.2 Frequency analysis

A Fast Fourier transform (FFT) with a moving Hanning-window was applied for 2 s segment and the frequency range was defined to be within the interval from 1 to 30 Hz. The auto-power spectral density matrices were averaged through the segments for every subject and condition.

3.1.3 Statistics

For frequency from 1 to 30 Hz with around 1 Hz step normalizing power were subjected to nonparametric statistical test by calculating Monte-Carlo estimates of the significance probabilities including two steps: cluster-based test statistic and its significance probability as implemented in FieldTrip (http://fieldtrip.fcdonders.nl/). The Monte Carlo permutation test is a nonparametric statistical test which increases sensitivity and avoids the problem of multiple comparisons. In the first step for all samples (channel, frequency), the experimental conditions t-test was done. Selected samples were clustered in connected sets based on spatial and spectral adjacency. Cluster-level statistics were calculated by taking the sum of F-values within every cluster. The statistical comparisons were done with respect to the maximum values of the summed F-values. In the second step, the Monte Carlo significance probability was calculated

for found clusters with within-subjects experimental designs. The clusters were considered significant if its p-value was less than 0.05. For the computation of Monte Carlo approximation, a permutation test was conducted, i.e., randomizing data across 2 conditions and rerunning the statistical test 1000 times, we obtained a reference distribution of the maximum of summed cluster F-values to evaluate the statistic of the actual data.

3.1.4 Two-way ANOVA

After the preprocessing step, signal processing was continued using the Fieldtrip toolbox.

A two-way repeated-measures ANOVA was used to establish if there was a statistically significant effect within main factors, group and time and their interaction for each frequency band. Four frequency band were selected: delta 1-3 Hz, theta 4-7 Hz, alpha 8-12 Hz and beta 13-30 Hz. The time factor included two-time intervals pre-ictal/pre-interictal and during ictal/during-interictal. The group factor consisted of ictal and interictal abnormal EEG activity. The respective power spectra were averaged in each frequency band.

Generally, the ANOVA test tells whether there is an overall difference between the groups (in means) and statistically significant results indicate that not all of the group means are equal (Suckling & Bullmore, 2004). However, it does not give the information which specific group differs. As ANOVA shows a significant difference between groups, then pot hoc test is applied to explore differences between the group means.

When ANOVA showed significant differences for main factors or their interactions, then a post-doc test was applied for significant effects to explore whether there was an increase or decrease in activity and what was the magnitude of those differences.

The sensor level results with statistics were visualized in Fieldtrip using the function ft_topoplotER.

3.2 Source-level connectivity analysis

Pre-processed EEG data were used for source-level connectivity analysis. For the source localization, the above-mentioned forward and inverse solutions were conducted using the open-source toolboxes METH (https://www.nitrc.org/projects/meth/) and Fieldtrip (Oostenveld et al., 2003), both for non-normalized and normalized EEG data.

3.2.1 The EEG Forward Problem

As there were no individual brain MR images available, the head was modelled by a realistic head model consisting of 3 layers (scalp, skull and brain). The geometries of these head tissues were segmented from a T1-weighted standard MRI (Colin 27). The conductivities of the head compartments were taken from the literature. The solution of the EEG forward problem was performed numerically via the boundary element method (BEM) (Oostenveld et al.,2003). Afterwards, the lead field matrix (LFM) was calculated in the METH toolbox. First, the structural calculation was performed, which includes information about the volume conductor and the electrode positions. For electrode positions, the standard Montreal Neurological Institute (MNI) coordinates were used. After completing LFM calculation for grid options, the medium grid size of the 3 types of grids was selected. The selected medium grid size contains 5003 points with 7.5 mm grid resolution, i.e. the distance between neighboring nodes. The node, or grid point, corresponds to grid point possible location of a current dipole with three directions x, y and z.

3.2.2 The EEG Inverse Problem

The inverse solution starts with the construction of a spatial filter based on eLORETA (Pascual-Marqui, 2011). The weights of the spatial filter were calculated for each grid point in all three orthogonal dipole directions.

Following this, the cross-spectral matrix was calculated for surface EEG data in METH toolbox for 1-second-long segments and was estimated for frequencies from 1-30 Hz with 1-Hz steps. The results were averaged over EEG segments and for four frequency bands (Delta, Theta, Alpha, and Beta).

Using the function getdipdir from the METH toolbox, the 3-dimensional filter was used on the cross-spectral matrix in the sensor space to determine the source orientation for each grid point. Consequently, the dipole orientation that maximizes the source power was calculated.

As a result, we obtained the source power, the dipole direction and a 1-dimensional filter at each grid point. This process projects the sensor-level, or surface EEG, into the brain to estimate the source activity.

To analyze the source results statistically, the power spectra from the ictal and interictal discharges were compared via the two-way repeated-measures ANOVA in the Fieldtrip toolbox. This analysis is based on the Monte-Carlo method, which is a non-parametric

permutation test with cluster correction to solve the multiple comparisons problem. As a result, the source activity for ictal and interictal discharges was statistically differentiated.

The final step, visualization, was performed also in Fieldtrip, which comprises interpolation of the source analysis results and statistical maps onto the grid points and then overlaying the results on the anatomical MRI. The mask from the statistics, the same as generated significant p-value (p<0, 05) was used for this interpolation. For anatomical labelling the Automated Anatomical Labelling (AAL) Atlas was utilized (Tzourio-Mazoyer et al.,2002). Consequently, the results were visualized using 2D axial slices of the brain on which the functional data are plotted. Additionally, the slices that contain three orthogonal directions (axial, sagittal and coronal) are shown.

3.3 Steps for Functional connectivity

The source maximum (MNI max), obtained from time effect after source analysis, was defined as a seed-reference region. For the seed selection of the source maximum, the MNI coordinates were used. For connectivity estimation, the imaginary part of coherency (iCoh) was used.

The connectivity was calculated based on the coherence of the seed grid point and all other grid points in the brain.

Connectivity analysis was performed for each of the four frequency bands (delta, theta, alpha and beta).

For the calculation of the imaginary part of coherency (iCoh) (in METH toolbox), initially, the 1-dimensional filter was used to calculate the cross-spectra at the source level. Secondly, the coherence from the cross-spectrum was calculated at the source level. Consequently, the coherency matrix was constructed which contained the real and imaginary part of coherency at the source level. The matrix was used to extract the coherency value corresponding to the seed and accordingly the absolute value of the imaginary part was chosen.

To assess the statistical significance of the connectivity results, the two-way repeated-measures ANOVA was used. Then for the significant ANOVA results, post hoc test was applied.

Finally, iCoh results with statistics were visualized on 2D axial slices of the brain and in orthogonal slices of the brain containing three directions (views) (axial, sagittal and coronal). The Anatomical labelling (AAL) atlas was used for the anatomical labelling.

4. Results

4.1 Sensor-level analysis results

Two-way repeated ANOVA revealed significant time effect over all channels for all frequency bands (except occipital channels for alpha and beta bands). It did not show a significant effect on the group and interaction levels. Post-hoc test for main time effect revealed that epochs with EEG discharges (during ictal/interictal) have higher power compared to epochs before the discharges (pre-ictal/interictal) in all frequency bands. The maximal power differences were mostly localized in the frontal and temporal regions.

a. ANOVA for the delta Band showed significant difference ($p=0.000999$) in all channels (except O2).
   Post hoc test displayed the greatest power difference ($p=0.000999$) was located in Frontal (F3, Fz, F4, FC1, FC2) region and second strongest power was detected in right temporal and anterior frontal regions (FT10, T4, Fp1, Fp2) (Figure 3).

b. ANOVA for theta Band showed significant difference ($p=0.001998$) in all channels (except F4, T3).
   Post hoc test, gave the greatest power difference ($p=0.000999$) located in fronto-central (FC1, FC2) region and the second strongest power located in right temporal region (FT10, T4). After Post hoc test F3, Fz, F4 areas were lost (cancelled out) (Figure 4).

c. ANOVA for alpha Band showed significant difference ($p=0.000999$) in all channels (except O2).
   Post hoc test, displayed that the greatest power difference ($p=0.000999$) was located in Frontal (Fp1, Fp2, F3, Fz, F4) region and second strongest power was detected in right temporal region (FT10) (Figure 5).

d. ANOVA for beta Band showed significant ($p=0.000999$) difference in all channels (except O1, O2).
   Post hoc test, displayed that the greatest power difference ($p=0.000999$) was located in Frontal (F3, Fz, F4) region and second strongest power was detected in further frontal and right temporal regions (Fp1, Fp2, FC1, FC2, FT10) (Figure 6).

Figure 3. Two-way ANOVA results and post hoc test for delta band

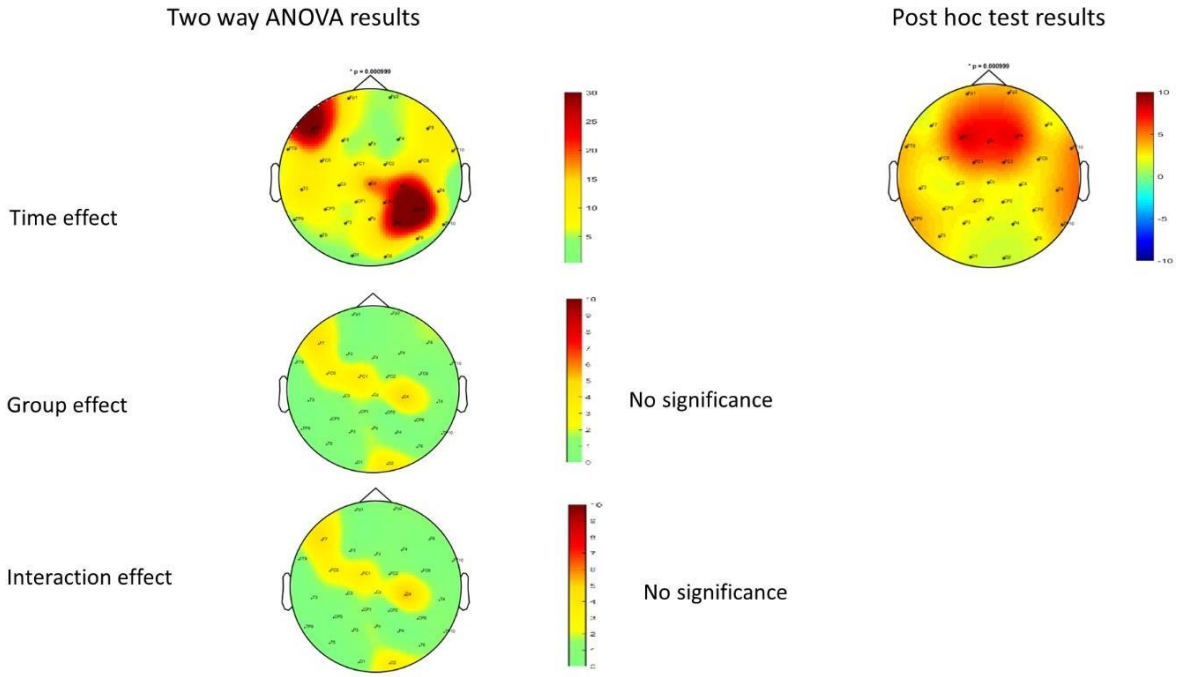

Figure 4. Two-way ANOVA results and post hoc test for theta band

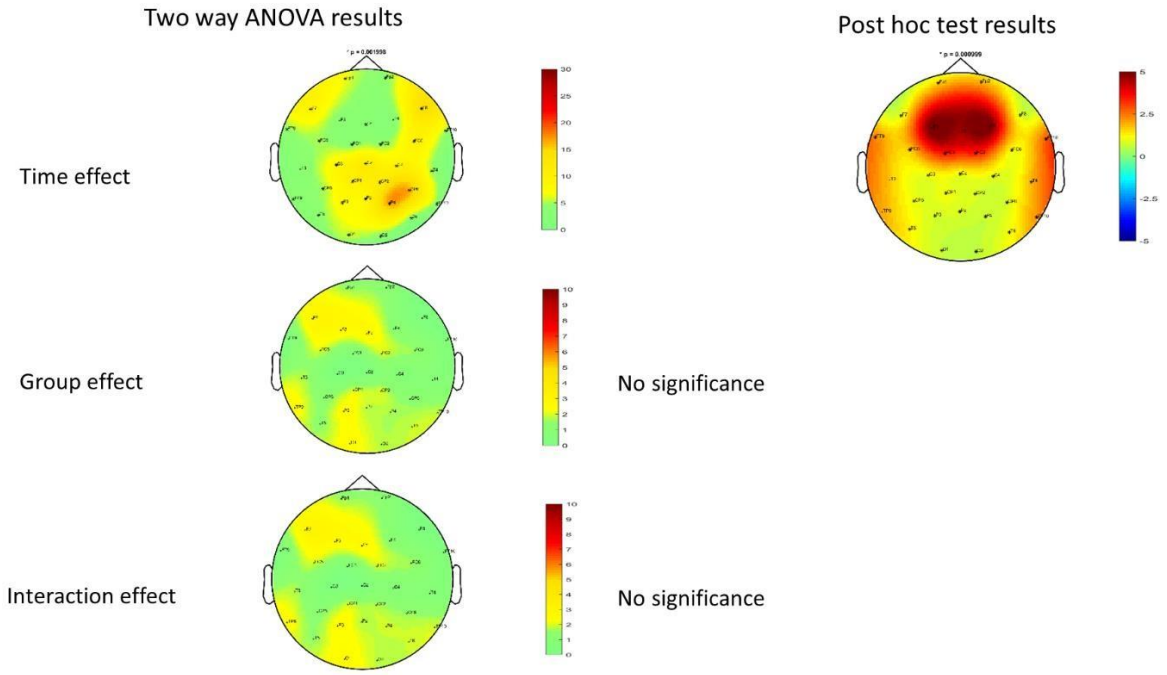

Figure 5. Two-way ANOVA results and post hoc test for alpha band

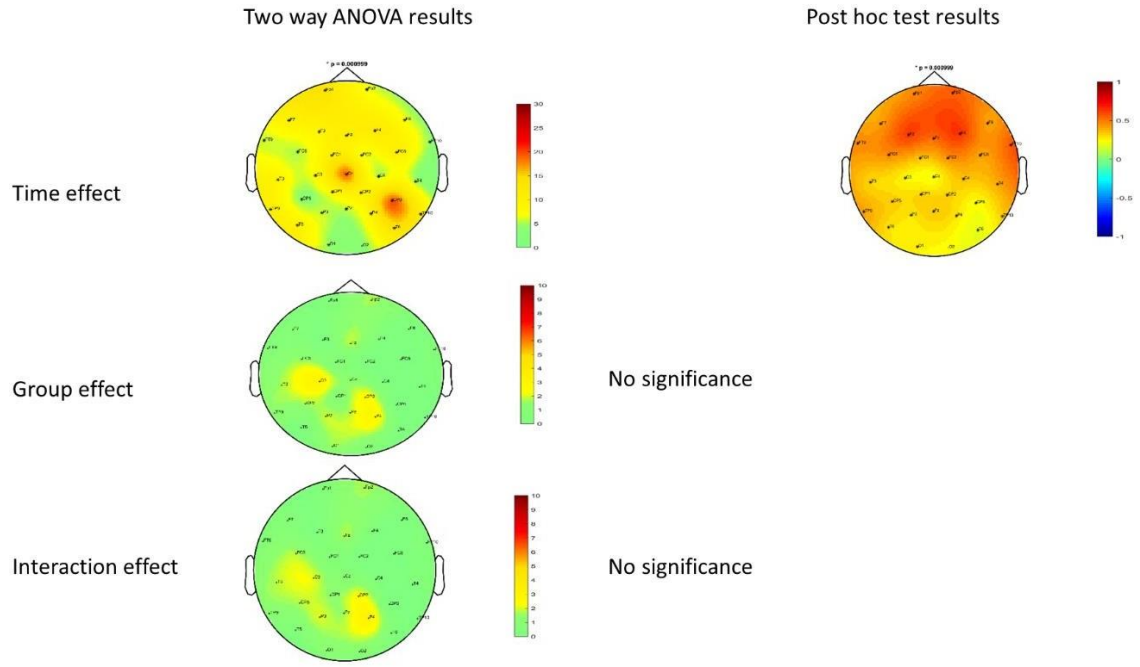

Figure 6. Two-way ANOVA results and post hoc test for beta band

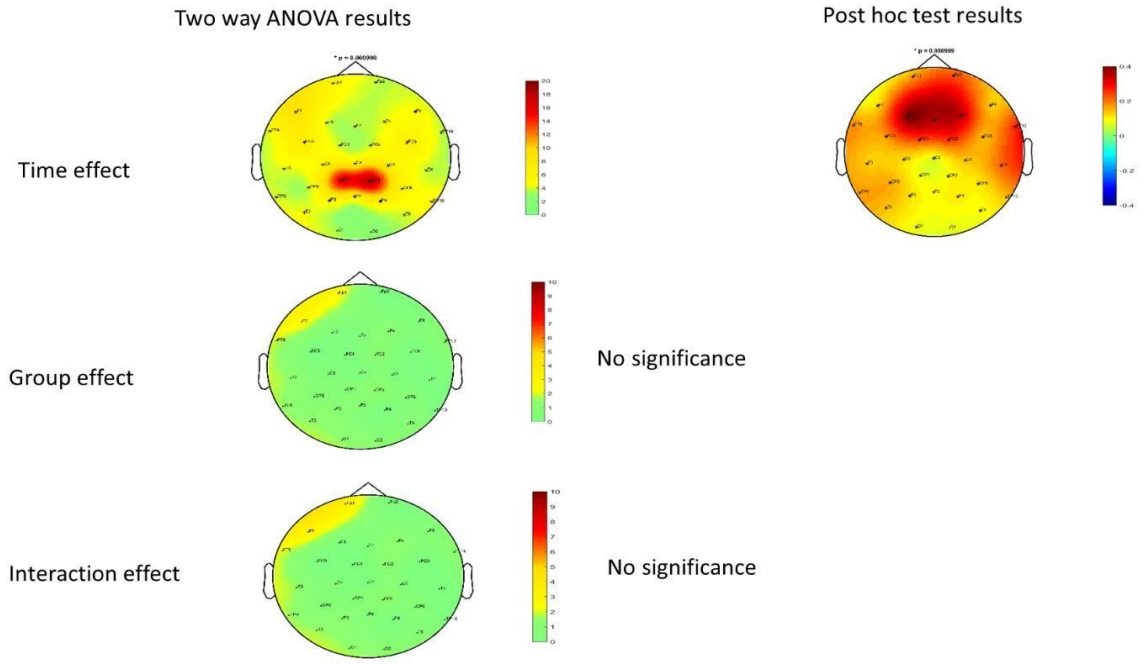

4.2 Source level analysis results

The group-level analysis on the source level was performed for both normalised and non-normalise data. As there was no significant difference found between the results of these two conditions (normalised vs non-normalised), we decided to put the normalised data for the main results. The results of the non-normalized data will be included in the supplementary material.

4.2.1 Source results for normalised data:

a. Delta Bend

For the delta band, two-way repeated measure ANOVA showed no significant group effect or interaction effect. It showed a significant time effect with the source of the strongest power in the right occipital region (the right calcarin gyrus), mni coordinates [28.0 -56.0 12.0] mm. Posthoc test for time effect revealed that during ictal/interictal segments had a stronger source power compared to pre-ictal/interictal segments. The significant difference with a maximum of powerbetween during ictal/interictal intervals and pre- ictal/interictal intervals was localised in left frontal rectus gyrus; (mni coordinates [-2.0 12.0 -26.0] mm) (Figure 7).

b. Theta band

Two-way repeated ANOVA for the theta band showed a significant time effect. The strongest power was seen in the right parietal lobe (the right parietal inferior gyrus and right supramarginal gyrus); mni coordinates [58.0 -32.0 50.0] mm. After applying post hoc test thesignificant source maximum was localised in the left frontal rectus gyrus (mni coordinates [- 2.0 20.0 -32.0] mm) (Figure 8).

c. Alpha band

The ANOVA result for the alpha band showed the strongest power in the right occipital region(the right cuneus), mni coordinates [12.0 -92.0 42.0] mm. After performing the post hoc test for time effect the source of maximal power showed no label (NA) (mni coordinates [-2.0 20.0 - 32.0] mm). The closest strongest label was the right frontal rectus gyrus (mni coordinates [4.0 28.0 -26.0] mm) (Figure 9).

d. Beta band

The two-way repeated ANOVA for the beta band again gave only the significant time. There was no significant difference found for group and interaction effect. The strongest

power was detected in the right parietal lobe (right superior parietal gyrus), mni coordinates [28.0.-78.0 58.0] mm. The post hoc test showed the strongest source power localised in the right and left frontal rectus gyri (mni coordinates [4.0 28.0 -26.0] mm) (Figure 10).

Figure 7. Source results for the delta frequency band

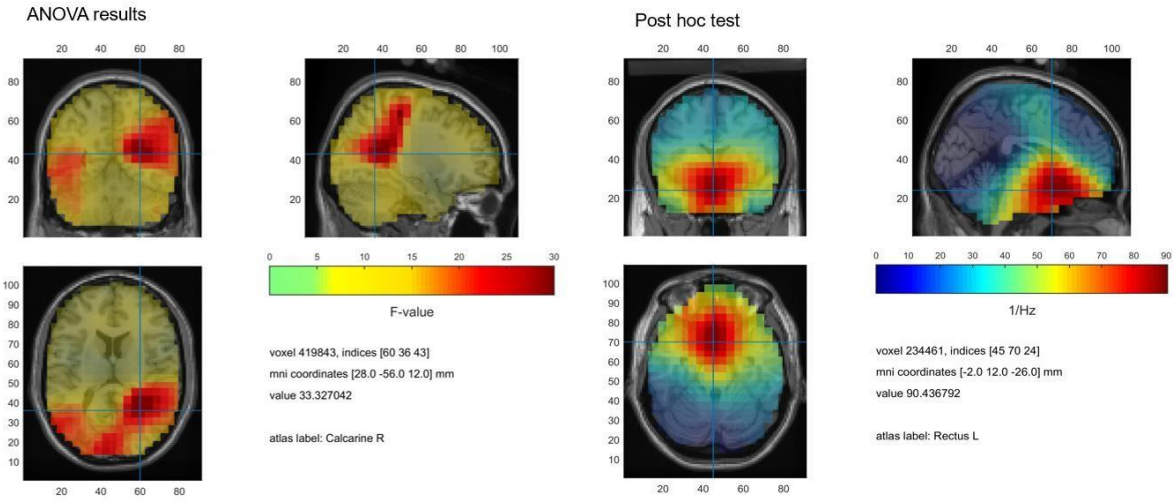

Figure 8. Source results for the theta frequency band

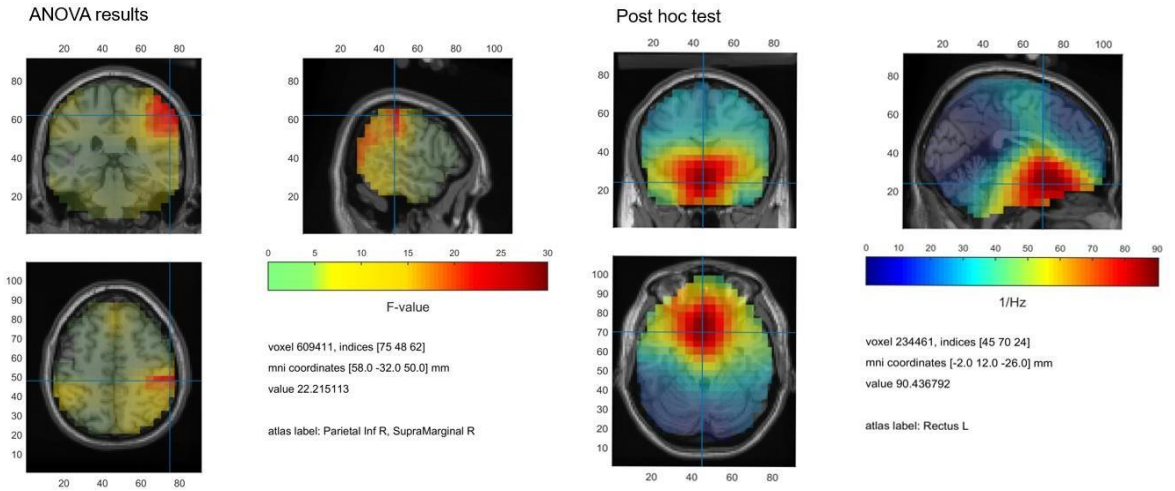

Figure 9. Source results for the alpha frequency band

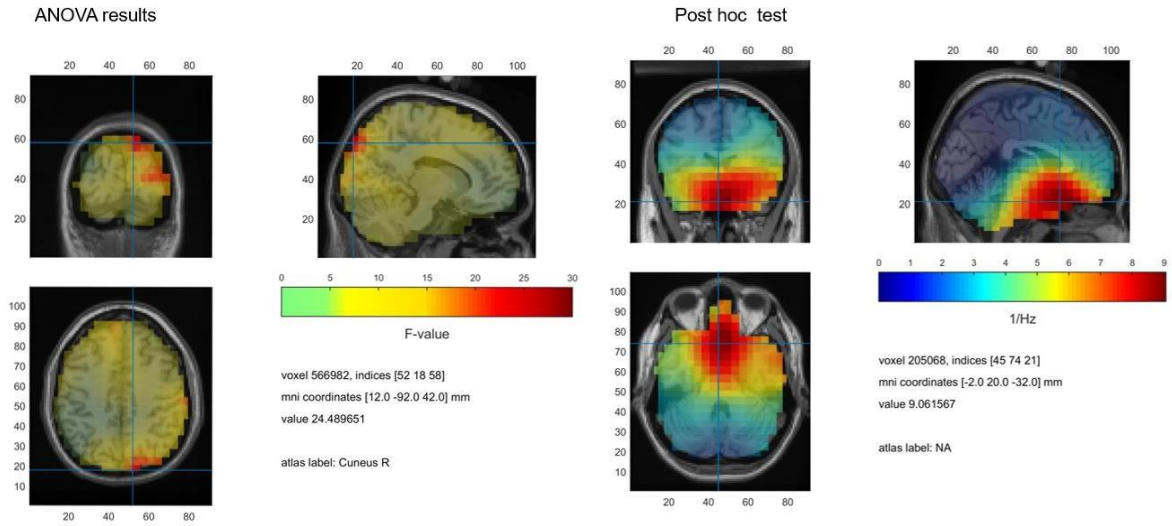

Figure 10. Source results for the beta frequency bend

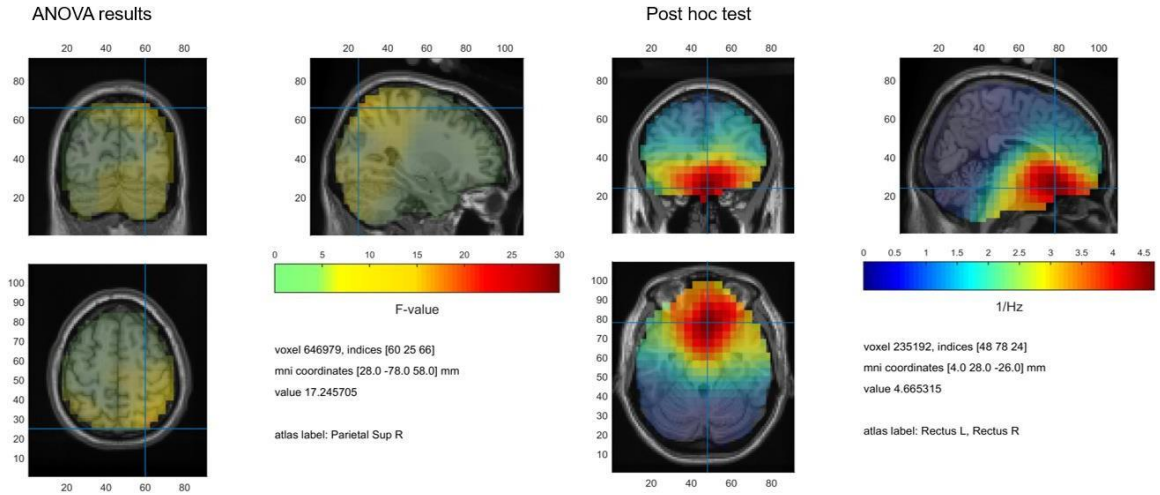

4.2.2 The imaginary part of coherency using source maximum as a seed

Comparison of imaginary part of coherency (iCoh) for all four-frequency bands ANOVA showed significant time effect (except for alpha band). For group and interaction, effect there was no significant difference found in any bands.

Post-hoc test for the time effect showed that during ictal/ interictal intervals have higher iCoh compare with pre-ictal/interictal intervals in three (delta, theta, beta) frequency bands.

a) For the delta band, the strongest coherence with the source maximum (left rectus gyrus) was detected in the right angular gyrus and right supramarginal gyrus. Other coherent regions were the right superior temporal gyrus, right middle occipital gyrus, right inferior parietal gyrus, right rolandic operculum, right precuneus, right middle temporal, left middle cingulum, left precuneus, left inferior parietal gyrus, left postcentral gyrus, left superior parietal gyrus. (Figure 11, Table 2)

b) At the theta frequency band, the strongest coherent region for the source maximum (left rectus gyrus) was localised in the left Angular gyrus. Other coherent regions were the right angular gyrus, left inferior parietal gyrus, left superior parietal gyrus and left postcentral gyrus, followed by left middle cingulum, left precuneus, left precentral gyrus, left inferior parietal gyrus, right precuneus, left posterior cingulum (Figure 12, Table 2).

c) For the alpha band, ANOVA did not show significance difference for time effect, neither for group nor for interaction effect.

d) For the beta band, the strongest coherence with the source maximum (right and left rectus gyrus) was detected in the right angular gyrus. Other coherent regions were right middle occipital, right inferior parietal, right superior temporal, right middle temporal, left postcentral, left rolandic operculum, left superior temporal, left supramarginal, left supplementary motor area, left superior frontal, right precuneus, left precentral, left middle cingulum, right middle cingulum, left superior middle frontal, right superior middle frontal, right cuneus, right calcarine, left middle frontal, left and right anterior cingulum (Figure 14, Table 2).

Figure 11. The imaginary part of coherency for the delta frequency band

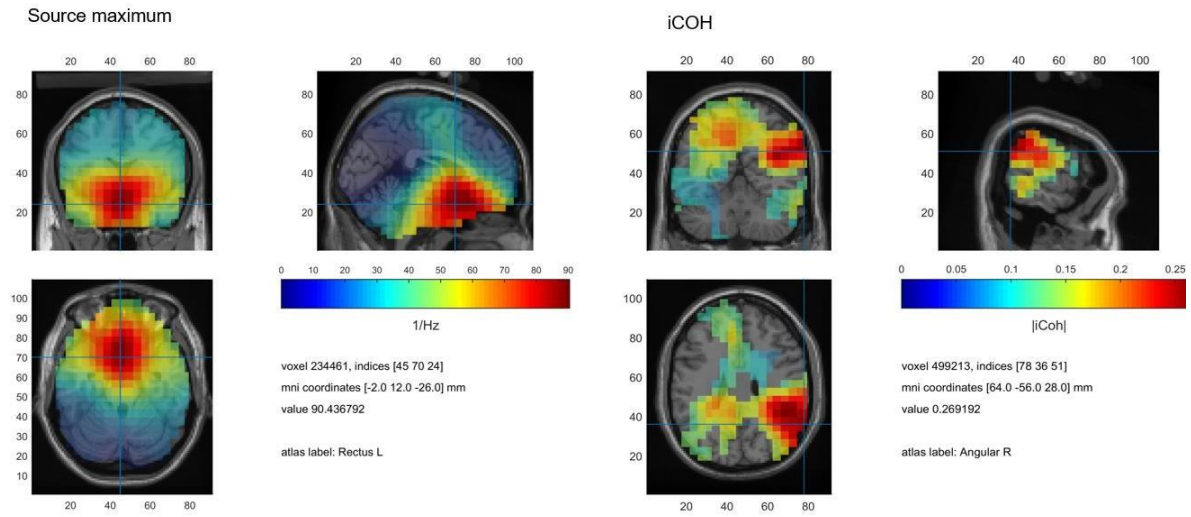

Figure 12. The imaginary part of coherency for the theta frequency band

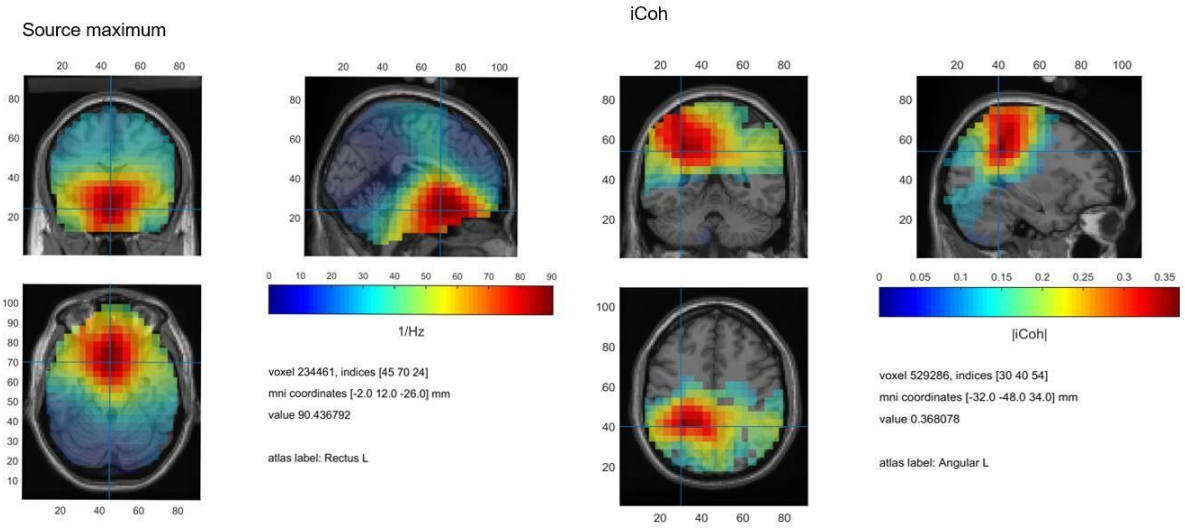

Figure 13. The imaginary part of coherency for the alpha frequency band

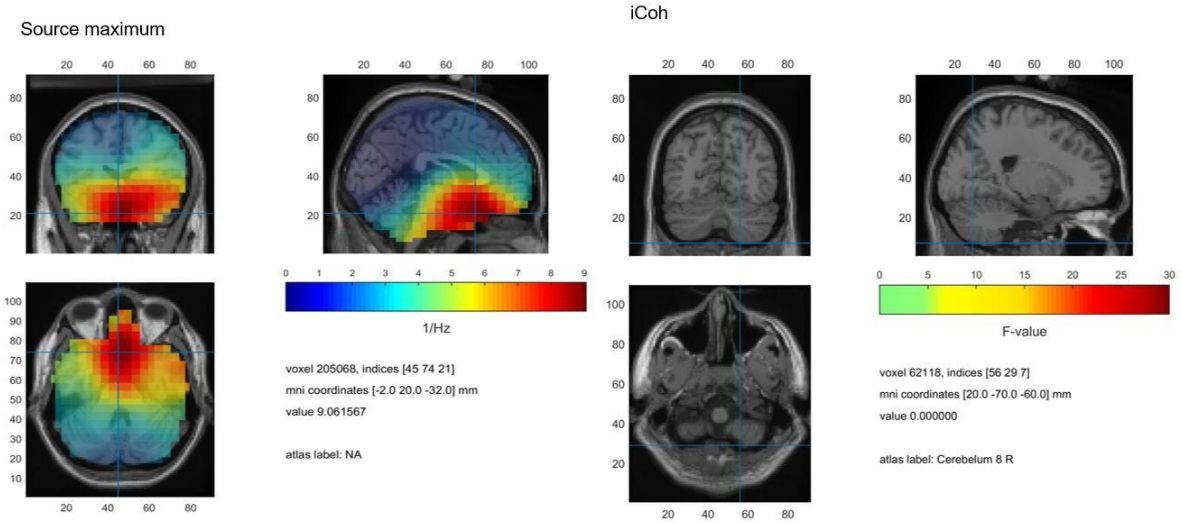

Figure 14. The imaginary part of coherency for the beta frequency band

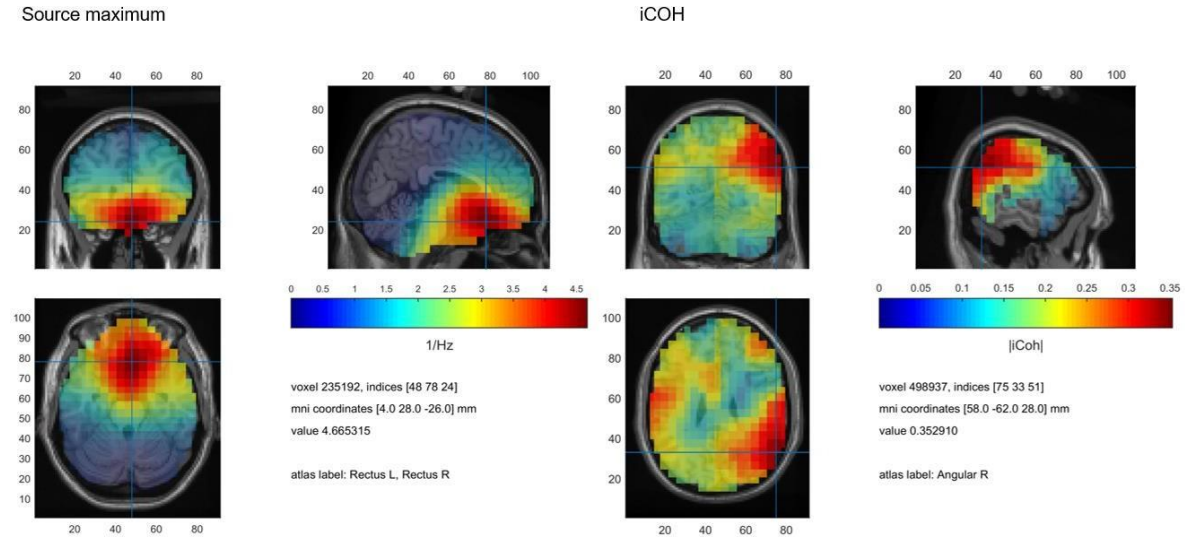

Table 2. Coherent regions with the source maximum for the normalized data

Frequencyband	Atlas label	Value
Delta band	Right angular gyrus	0.269192
	Right supramarginal gyrus	0.269192
	Right middle occipital gyrus	0.251854
	Right superior temporal gyrus	0.251854
	Right inferior parietal gyrus	0.236782
	Right precuneus	0.236950
	Right rolandic operculum	0.232789
	Right middle temporal gyrus	0.226989
	Left middle cingulum	0.211000
	Left precuneus	0.211303
	Right parietal inferior gyrus	0.207468
	Left parietal inferior gyrus	0.203592
	Left postcentral gyrus	0.205022
	Left parietal superior gyrus	0.205022
Theta band	Right angular gyrus	0.368078
	Left parietal inferior gyrus	0.368078
	Left middle cingulum	0.348481
	Left precuneus	0. 348481
	Left postcentral gyrus	0.341724
	left superior parietal gyrus	0.338873
	Left precentral gyrus	0.283826
	Right Angular gyrus	0.352919
	Right middle occipital gyrus	0.340036
	Right inferior parietal gyrus	0.336940
	Right superior temporal gyrus	0.325725
	Right middle temporal gyrus	0.318550
	Left postcentral gyrus	0.304785

	Left rolandic operculum	0.306686
Beta band	left superior temporal gyrus	0.304785
	Left supramarginal gyrus	0.290246
	Left supplementary motor area gyrus	0.284862
	Left superior frontal gyrus	0.284862
	Right precuneus gyrus	0.270583
	Left precentral gyrus	0.262263
	Left middle cingulum gyrus	0.255659
	Right middle cingulum	0.255659
	Left superior middle frontal gyrus	0.258531
	Right superior middle frontal gyrus	0.258531
	Right cuneus	0.259487
	Right calcarine	0.255228
	Left middle frontal gyrus	0.251140
	Left, right anterior cingulum	0.231494

4.2.3 The imaginary part of coherency using thalamus as a seed

ANOVA test of imaginary part of coherency for all frequency bands using thalamus as a seed showed significant time effect (except for alpha band). For group and interaction effects, no significant difference was detected in any bands.

Post-hoc test analysis for time effect showed that during ictal/interictal intervals have higher iCoh in three (delta, theta, beta) frequency bands in comparison to pre-ictal/interictal intervals.

1. Delta band showed that the strongest coherent source with thalamus was located in the right supramarginal gyrus, followed by the right supramarginal gyrus, right angular gyrus, right superior temporal gyrus, right postcentral gyrus, left postcentral gyrus, right cuneus gyrus, right middle cingulum gyrus, left paracentral lobule gyrus, right middle occipital gyrus, right middle temporal gyrus, right lingual gyrus, right inferior occipital gyrus, right calcarine, right superior occipital gyrus, right superior parietal gyrus, right inferior parietal gyrus, left supplementary motor area, left superior frontal gyrus, left medial frontal gyrus, left precuneus, right precentral gyrus, left posterior cingulum, left superior parietal gyrus, left inferior parietal gyrus, left middle cingulum and right precuneus gyrus (Figure 15, Table 3).
2. Theta frequency showed the strongest coherent source in the left parietal superior gyrus, followed by right angular gyrus, left parietal inferior gyrus, left middle cingulum, left precuneus, left postcentral gyrus, left superior parietal gyrus, left precentral gyrus (Figure 16, Table 3).
3. Alpha band showed no significant effects.
4. Beta band showed the strongest connection with the right angular gyrus, followed by right middle occipital gyrus, right inferior parietal gyrus, right superior temporal gyrus, right middle temporal gyrus, left postcentral gyrus, left rolandic oper gyrus, left superior temporal gyrus, left supramarginal gyrus, left supplementary motor area gyrus, left superior frontal gyrus, right precuneus gyrus, left precentral gyrus, left middle cingulum gyrus, right middle cingulum, left superior middle frontal gyrus, right superior middle frontal gyrus, right cuneus, right calcarine, left middle frontal gyrus, left, right anterior cingulum (Figure 17, Table 3).

Figure 15.The imaginary part of coherency using thalamus as a seed for the delta band

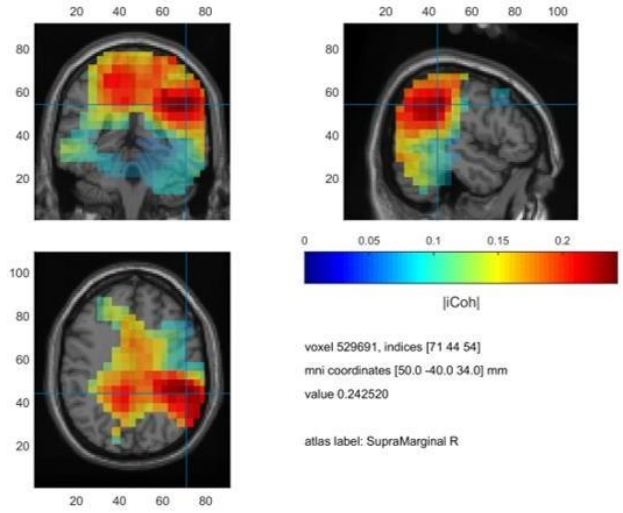

Figure 16. The imaginary part of coherency using thalamus as a seed for the theta band

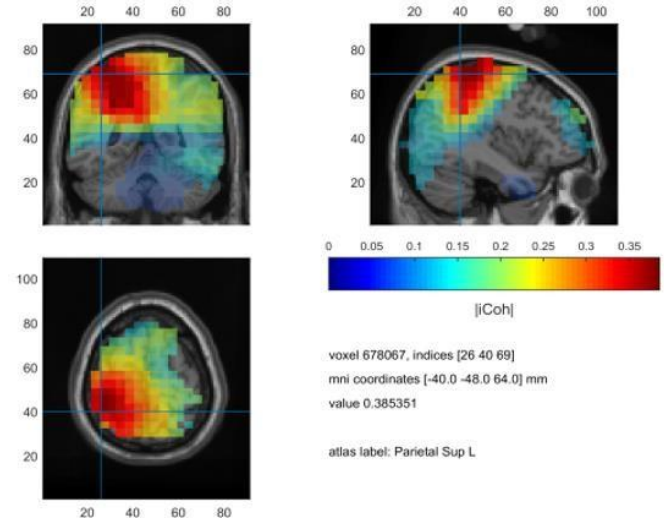

Figure 17. The imaginary part of coherency using thalamus as a seed for the beta band

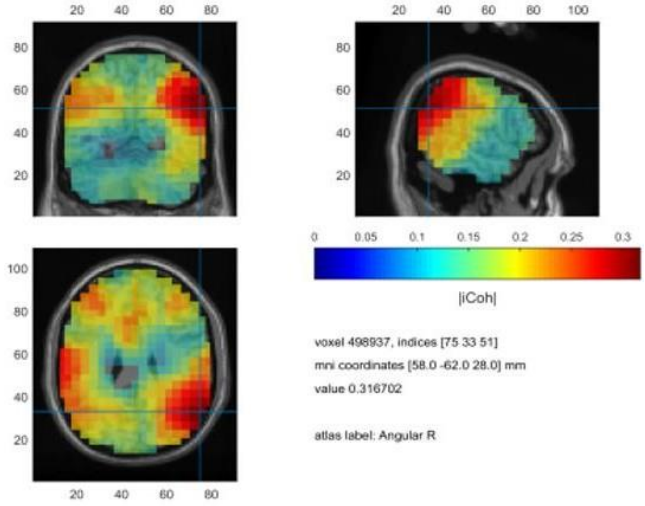

Table 3. Coherent regions with the thalamus for the normalized data

Frequencyband	Atlas label	Value
Delta band	Right supramarginal gyrus	0.242520
	Right angular gyrus	0.232554
	Right superior temporal gyrus	0.232554
	Right postcentral gyrus	0.233424
	left postcentral gyrus	0.210713
	Right cuneus gyrus	0.212907
	Right middle cingulum gyrus	0.212011
	Left paracentral lobule gyrus	0.204484
	Right middle occipital gyrus	0.217222
	Right middle temporal gyrus	0.202565
	Right lingual gyrus	0.204792
	Right inferior occipital gyrus	0.201483
	Right calcarine	0.199910
	Right superior occipital gyrus	0.194077
	Right superior parietal gyrus	0.194851
	Right inferior parietal gyrus	0.194851
	Left supplementary motor area	0.190551
	Left superior frontal gyrus	0.190551
	Left medial frontal gyrus	0.190551
	Left precuneus	0.199791
	Right precentral gyrus	0.195600
	Left posterior cingulum	0.182695
	Left superior parietal gyrus	0.181407
	Left inferior parietal gyrus	0.181407
	Left middle cingulum	0.186868
	Right precuneus gyrus	0.188998
	Left superior parietal gyrus	0.385351

	Left postcentral gyrus	0.385351
Thet a Ban d	Left parietal inferior gyrus	0.381235
	Left precentral gyrus	0.373033
	Left middle cingulum	0.367945
	Left precuneus	0.367945
	Right precuneus	0.332965
	Left angular gyrus	0.332632
	Left posterior cingulum	0.313523
Beta band	Right angular gyrus	0.316702
	Left postcentral	0.314917
	Right middle occipital	0.302774
	Right middle temporal	0.302774
	right superior temporal	0.299784
	Left supramarginal	0.291508
	Right inferior parietal	0.280524
	Right supramarginal	0.280524
	Left superior temporal	0.286203
	Left rolandic operculum	0.279455
	Left middle temporal	0.267058
	Left precentral	0.260603
	Left middle frontal	0.249310
	Left middle inferior frontal	0.234345
	Left heschl	0.235053
	Left angular	0.236510
	Right cuneus	0.231943
	Right calcarine	0.231943
	Right occipital superior	0.231439
	Right precuneus	0.231439
	Left superior frontal	0.239347
	Left superior medial frontal	0.239347
	Right middle cingulum	0.220912

	Right middle frontal	0.225755
	Left insula	0.224927
	Left middle occipital	0.214337
	Right postcentral	0.214861
	Right lingual	0.218849
	Right cerebellum	0.215582
	Right inferior occipital	0.218849

5. Discussion

The focus of this study was to describe neuronal networks underlying ictal (myoclonic) as well as interictal GSW EEG discharges in patients with Jeavons Syndrome (JS).

The analysis was carried out at both the sensor and the source level. On the sensor level the study aimed to investigate differences in the topographic distribution of EEG spectral power between eye closure induced ictal discharges and interictal EEG discharges. Even though there is a big clinical difference between ictal and interictal segments, we still could not find any significant difference in frequency power between these two groups. However, the power difference between ictal and preictal segments for four frequency bands was localized in frontal and temporal lobes.

On the source level we used eLORETA algorithm to identify sources underlying ictal and interictal EEG paroxysms for four-frequency bands. There were no significant group differences found between these two groups of segments. The identified sources were located in frontal rectus gyrus for all frequency bands. This area does not correspond to any known functional region (Joo MS et al., 2016). As eLORETA is not precise instrument to localize deep sources, we presume that received frontal rectus gyrus is shifted deep brain source from the thalamus. In order to prove this hypothesis we performed the following simulation. We placed the seed in thalamus and using iCoh performed FC analysis. Results of FC were compared to the FC results from the source in frontal rectus gyrus. In both cases, we received identical networks with involvement of the following structures listed by the strength:

a. For delta band the coherent regions for the source maximum were right angular and right supramarginal gyrus, followed by right superior temporal gyrus, right middle occipital gyrus, right inferior parietal gyrus, right rolandic operculum, right precuneus, right middle temporal, left middle cingulum, left precuneus, left inferior parietal gyrus, left postcentral gyrus, left superior parietal gyrus.
b. For theta band the most coherent regions for the source maximum were right angular gyrus, left inferior parietal gyrus, left superior parietal gyrus and left postcentral gyrus, followed by left middle cingulum, left precuneus, left precentral gyrus, left inferior parietal gyrus, right precuneus, left angular gyrus, left posterior cingulum.

c. For beta band the most coherent areas with the source maximum were right angular gyrus, right middle occipital, right inferior parietal, right superior temporal, right middle temporal, left postcentral, left rolandic operculum, left superior temporal, left supramarginal, left supplementary motor area, left superior frontal, right precuneus, left precentral, left middle cingulum, right middle cingulum, left superior middle frontal, right superior middle frontal, right cuneus, right calcarine, left middle frontal, left, right anterior cingulum

d. For the alfa band we did not find any significant effect of FC for both seeds.

The comparison of the value of functional connectivity between ictal and interictal discharges on source level did not give any significant difference.

The functional connectivity result shows thalamus connected to different regions of default mode of network (DMN) and involvement of areas of sensory-motor network and visual network accordingly to three different frequency bands.

5.1 Thalamus and DMN role in JS and IGE

We presume that the main source underlying GSW discharges in JS patients is thalamus, with maximal coherency with DMN regions. Our results are in concordance with previous FC studies performed on EMA (eyelid myoclonia with absences) and IGEs patients using EEG-fMRI, showing thalamus to be the main source, with connection to the regions of DMN (Vaudano et al., 2014; Liu et al., 2008).

Vaudano et al saw the BOLD signal changes in posterior thalamic nuclei (pulvinar), which participates in the control of visual attention (Fischer et al., 2012), information flow from and to the primary visual cortex (Purushothaman et al., 2012). It is the main component in generation of alpha rhythm together with parietal-occipital cortex and temporal cortices (Zou et al., 2009; Liu et al., 2016). Vaudano and colleagues proposed the hypothesis that abnormal activation of thalamus together with visual cortex is the exact pathogenesis of eye closure sensitivity (Vaudano et al., 2014; Duncan, 1996; Sevgi et al., 2007).

Liu et al analyzed ictal and interictal GSW activity of EMA patients, using EEG fMRI. They also found the predominant activation of BOLD signal in thalamus and deactivation of the region of DMN (Liu et al., 2008).

Also the previous fMRI studies in IGE group showed that thalamus and default mode areas are

involved in the pathogenesis of GSW paroxysms (Salek-Haddadi et a., 2003; Aghakhani et al., 2004; Gotman et al., 2005; Labate et al., 2005; Hamandi et al, 2006; Laufs et al, 2006; Moeller et al., 2009). In all groups, positive BOLD signal mainly was found in thalamus whereas a negative BOLD signal was localized in posterior cingulate, precuneus and bilateral parietal regions (Pugnaghi et al., 2014).

Study on small group of patients with CAE (Li et al., 2009) compared BOLD signal patterns during interictal and ictal discharges. They found similar cortical and subcortical networks during brief and long GSWDs. Positive BOLD signal was mainly located in thalamus whereas negative BOLD was found lateral parietal cortex, posterior cingulate gyrus, caudate nucleus.

In children with IGE, Moeller et al found that GSWs were associated with positive BOLD signals in a bilateral medial part of the thalamus, while the negative BOLD was found in fronto-parietal areas including precuneus. It is suggested that DMN areas such as parietal cortex, precuneus/posterior cingulate and prefrontal cortical areas active at rest and support the waking state of consciousness (Raichle et al., 2001). According to several fMRI studies DMN regions deactivate during epileptic activity (Gotman et al., 2005; Laufs et al., 2006; Kobayashi et al., 2009; Blumenfeld et al., 2009).

5.2 The role of Sensory-motor cortex in generation of eyelid myoclonus

In our study, we have found the involvement of regions participating in saccades and eye pursuit movements (the parietal cortex, premotor cortex, middle temporal gyrus and anterior cingulate). Our results were concordant with the previous study of Vaudano and colleagues (2014), where they have found activation of the same structures in particular the parietal cortex adjacent to the intraparietal sulcus, which, together with premotor cortex is the main part of the network generating saccades (Jamadar et al., 2013, Pierrot-Deseilligny et al., 2004). Intraparietal sulcus is also involved in generation of photoparoxysmal response (Wilkins et al., 2004). It is suggested, that the rapid luminance changes due to eye closure can trigger high frequency synchronization in the parietal cortex, that in turn propagates to the central motor cortex and frontal areas to generate the eyelid myoclonus, as demonstrated in patients with photic cortical reflex myoclonus (Rubboli et al., 1995). Vaudano et al also found abnormality in bilateral pericentral cortex adjacent to frontal eye field in EMA group, which is involved in saccade generation. The dysfunction of frontal eye field already has been described in photosensitive patients (Siniatchkin et al., 2007; Moeller et al., 2009). The fMRI study of Moeller et al showed the activation of the same areas (frontal eye field and intraparietal cortex) during the PPR (Moeller et al., 2009). We also found the involvement of middle temporal cortex, which is

known to be the major cortical hub for the control of smooth pursuit eye movements (Ruff et al., 2013; Hohl et al., 2013). Further on, we have found the involvement of cingulate, which together with mesial frontal region and fronto-opercular area control eye blinking (Morecraft et al., 2001).

Further studies on myoclonic seizures have also found association of abnormally increased synchronization in the frontal motor and premotor cortices (Oguni et al., 1994; Panzica et al., 2001). Sensorimotor involvement and connectivity alterations of these regions has already been described in other studies on myoclonic seizures and benign epilepsy with centro-temporal spikes (Brindley et al., 2016; Hamandi et al., 2011; Manganotti et al.,2004).

The most broadly studied form of idiopathic myoclonic epilepsy is JME. Previous studies have discussed that JME could be a brain network disorder with predominately medial frontal cortex and the posterior cingulate involvement (O'Muircheartaigh et al., 2011; Kim et al 2012). The FC connectivity studies of the background activity on the patients with myoclonic seizure from IGE group showed functional abnormalities of sensorimotor network (SMN) (Li et al., 2017); supplementary motor area (SMA) and primary motor cortex (Vulliemoz et al., 2011). Further, EEG-fMRI studies showed involvement of posterior brain regions, DM and subcortical brain areas during SWD in JME (Aghakhari et al., 2004; Hamandi et al., 2006; Gotmann et al., 2005) and precuneus, modulating these discharges (Vaudano et al., 2009).

Other fMRI studies have shown altered connectivity in JME involving thalamus, cerebellum, precuneus, inferior temporal lobe, and sensorimotor areas (including the middle cingulate cortex, supplementary motor area, paracentral lobule) (Qin et al., 2019; Zhong et al., 2018).

In the study of Clemens et al analysis of EEG segments of the patients with JME using LORETA and EEG-FC, where they compared immediate pre-ictal epochs to discharge free EEG segment, the significant difference was found only in delta band, with increase of delta hypercoupling between the posterior brain parts (cuneus, paracentral lobule and cingulate gyrus) (Clemens et al., 2013). Also very recent study on JME showed increased connectivity in theta and alpha band also in posterior brain regions and decreased connectivity in pre- and postcentral (sensory-motor) brain regions (Routly et al ., 2020).

Increased connectivity among the motor and non-motor areas, temporal, parietal and occipital brain regions may explain the mechanism underlying the photic stimulation induced eyelid myoclonus (Clemens et al., 2013). Our results are in line with these connectivity studies on JME and especially myoclonic seizures.

5.3 Visual Network

Our results also showed the involvement of visual cortex, suggesting that abnormal occipital neuronal activity after eye closure gives rise to appearance of GSW discharges, which might persist through the patient's life. The involvement of bilateral calcarine gyrus (Vaudano et al., 2014) and occipital cortex (Viravan et al., 2011) in eye closure induced EEG discharged and photosensitivity phenomena has been already described, with either due to the hyperexcitability of visual cortex or impaired intracortical inhibition (Striano et al., 2009; Siniatchkin et al., 2007).

6. Conclusion

In this study, we have aimed to describe neuronal networks underlying ictal (myoclonic) as well as interictal GSW discharges in patients with JS. The clinical presentation of JS includes photosensitivity, together with eye closure sensitivity as a main trigger for the generalized polyspike and wave discharges proceeded with myoclonic seizures with to without absences. In our FC study, we found a complex involvement of different brain networks. We saw the thalamus connection to the brain regions, which participate in state of consciousness, oculomotor control, myoclonus, eye closure sensitivity and photosensitivity. Our result complies with the previous results of fMRI studies performed in JS and IGEs Patients.

However, when we compared the FC of ictal and interictal EEG Paroxysms we could not find any significant differences. This could be due to the fact that we only selected one seizure type, myoclonus and excluded epochs with absences. We speculate that the reason we did not see any group differences in DMN network is that the state of consciousness was not altered in the selected segments. Connected to the state of consciousness we could not get the difference between the groups.

However, in our study, using EEG source analyses we could describe networks involved in pathogenesis of JS previously demonstrated by numerous EEG fMRI studies.

Our study had several limitations: small group of patient, standardized head-models, low number of EEG channels, and various antiepileptic medications used during the EEG recordings.

7. References

Adachi M, Inoue T, Tsuneishi S, Takada S, Nakamura H. Eyelid myoclonia with absences in monozygotic twins. Pediatr Int 2005; 47(3): 343-7.

Adebimpe A, Aarabi A, Bourel-Ponchel E, Mahmoudzadeh M, Wallois F. EEG resting state functional connectivity analysis in children with benign epilepsy with centrotemporal spikes. Front Neurosci 2016; 10,143. doi.org/10.3389/fnins.2016.00143

Aghakhani Y, Bagshaw AP, Bénar CG, Hawco C, Andermann F, Dubeau F, Gotman J. fMRI activation during spike and wave discharges in idiopathic generalized epilepsy. Brain 2004; 127(5):1127-44. doi: 10.1093/brain/awh136.

Aoki Y, Ishii R, Pascuai-Marqui R D, Canuet L, Ikeda S, Hata M, Imajo K, Matsuzaki H, Musha T, Asada T, Iwase M, Takeda M. Detection of EEG-resting state independent networks by eLORETA method. Front Neurosci 2015; 1-2. doi.org/10.3389/fnhum.2015.00031

Arivo M, Sauna-Aho O, Nyrke T, Bjelogrlic-Laakso N. Intellectual disability in patients with epilepsy with eyelid myoclonias. SAGE Open Med Case Rep 2018: 21; 6:2050313X18777951. doi: 10.1177/2050313X18777951.

Bianchi A. Italian League Against Epilepsy. Studies of concordance of syndromes in families with absence epilepsies. In: Duncan J, Panayiotopoulos CP, Editors. Typical absence seizures and related epileptic syndromes. London: Churchill Livingstone, 1995; 328-37.

Blumenfeld H, Varghese GI, Purcaro MJ, Motelow JE, Enev M, McNally KA, Levin AR, Hirsch LJ, Tikofsky R, Zubal IG, Paige AL, Spencer SS. Cortical and subcortical networks in human secondarily generalized tonic-clonic seizures. Brain 2009;132(4):999-1012. doi: 10.1093/brain/awp028.

Brazier MA. Spread of seizure discharges in epilepsy: anatomical and electrophysiological considerations. Exp Neurol 1972; 36(2):263–72.

Brindley LM, Koelewijn L, Kirby A. Ipsilateral cortical motor desynchronisation is reduced in Benign Epilepsy with Centro-Temporal Spikes. Clin Neurophysiol 2016; 127(2):1147-1156. doi: 10.1016/j.clinph.2015.08.020.

Canuet L, Ishii R, Pascual-Marqui R D, Iwase M, Kurimoto R, Aoki Y, Ikeda S, Takahashi H, Nakahachi T, Takeda M. Resting-state EEG source localization and

functional connectivity in schizophrenia-like psychosis of epilepsy. PloS One 2011; 6 (11). doi.org/10.1371/journal.pone.0027863

Capovilla G, Striano P, Gambardella A. Eyelid fluttering, typical EEG pattern, and impaired intellectual function: a homogeneous epileptic condition among the patients presenting with eyelid myoclonia. Epilepsia 2009;50(6):1536-41.

Caraballo R H, Fontana E, Darra F, Chacon S, Ross N, Fiorini E, Fejerman N, Bernardina B D. A study of 63 cases with eyelid myoclonia with or without absences: Type of seizure or an epileptic syndrome? Seizure 2009; 18(6):440-5

Choi S. Independent component analysis. In Handbook of Natural Computing, 2012;1– 4: 435–459. Springer Berlin Heidelberg. doi.org/10.1007/978-3-540-92910-9_13

Clemens B, Puskás S, Besenyei M, Spisák T, Opposits G, Hollódy K, Fogarasi A, Fekete I, Emri M. Neurophysiology of juvenile myoclonic epilepsy: EEG-based network and graph analysis of the interictal and immediate preictal states. Epilepsy Res 2013; 106(3):357-69. doi: 10.1016/j.eplepsyres.2013.06.017.

Dressler O, Schneider G, Stockmanns G, Kochs E F. Awareness and the EEG power spectrum: Analysis of frequencies. B J Anaesth 2004; 93(6), 806–809. doi.org/10.1093/bja/aeh270.

Drongelen W, Yuchtman M, Vanveen B D, Vanhuffelen A C. A spatial filtering technique to detect and localize multiple sources in the brain. Brain Topogr 1996; 9:39- 49

Duncan JS, Panayiotopoulos CP. Eyelid myoclonia with absences. London: John Libbey and Company Ltd , 1996; 107-14

Elshoff L, Muthuraman M, Anwar A R, Deuschl G, Stephani u, Raethjen J, Siniatchkin

M. Dynamic imaging of Coherent Sources reveals different network connectivity underlying the generation and perpetuation of epileptic seizures. PLOS 2013; e78422

Engel J Jr. Report of the ILAE classification core group. Epilepsia. 2006; 47(9):1558- 68. doi: 10.1111/j.1528-1167.2006.00215.x.

Fisher RS, Cross JH, French JA. Operational classification of seizure types by the International League Against Epilepsy: position paper of the ILAE Commission for Classification and Terminology. Epilepsia 2017a; 58(4):522-30.

Fisher RS, Cross JH, D'Souza C. Instruction manual for the ILAE 2017 operational classification of seizure types. Epilepsia 2017b; 58(4):531-42.

Fischer J, Whitney D. Attention gates visual coding in the human pulvinar. Nat Commun 2012; 3:1051. doi: 10.1038/ncomms2054.

Fournier-Goodnight AS, Gabriel M, Perry MS. Preliminary neurocognitive outcomes in Jeavons syndrome. Epilepsy Behav 2015; 52(A):260-3.

Fries P. A mechanism for cognitive dynamics: Neuronal communication through neuronal coherence. TiCS 2005; 9(10), 474–480. doi.org/10.1016/j.tics.2005.08.011

Galizia EC, Myers CT, Leu C, de Kovel CG, Afrikanova T, Cordero-Maldonado ML, Martins TG, Jacmin M, Drury S, Krishna Chinthapalli V, Muhle H, Pendziwiat M, Sander T, Ruppert AK, Møller RS, Thiele H, Krause R, Schubert J, Lehesjoki AE, Nürnberg P, Lerche H; EuroEPINOMICS CoGIE Consortium, Palotie A, Coppola A, Striano S, Gaudio LD, Boustred C, Schneider AL, Lench N, Jocic-Jakubi B, Covanis A, Capovilla G, Veggiotti P, Piccioli M, Parisi P, Cantonetti L, Sadleir LG, Mullen SA, Berkovic SF, Stephani U, Helbig I, Crawford AD, Esguerra CV, Kasteleijn-Nolst Trenité DG, Koeleman BP, Mefford HC, Scheffer IE, Sisodiya SM. CHD2 variants are a risk factor for photosensitivity in epilepsy. Brain 2015;138 (5):1198-207.

García Domínguez L, Stieben J, Pérez Velázquez J, Shanker S. The imaginary part of coherency in autism: differences in cortical functional connectivity in preschool children. PloS one, 8(10), e75941. doi.org/10.1371/journal.pone.0075941

Giannakodimos S, Panayiotopoulos CP. Eyelid myoclonia with absences in adults: a clinical and video-EEG study. Epilepsia 1996; 37: 36-44.

Gotman J. A computer system to assist in the evaluation of the EEGs of epileptic patients. Behav Res Methods 1981; 13, 525–531.

Grech R, Cassar T, Muscat J, Camilleri KP, Fabri SG, Zervakis M, Xanthopoulos P, Sakkalis V, Vanrumste B. Review on solving the inverse problem in EEG source analysis. J Neuroeng Rehabil 2008; 7;5:25. doi: 10.1186/1743-0003-5-25.

Groening K, Brodbeck V, Moeller F, Wolff S, Van Baalen A, Michel C M , Jansen O, Boor R, Wiegand G, Stephani U, Siniatchkin M. Combination of EEG-fMRI and EEG source analysis improves interpretation of spike-associated activation networks in pediatric pharmacoresistant focal epilepsies. Neuroimage 2009; 46, 827-33.

Gross J, Kujala J, Hamalaonen M, Timmermann L, Schitzler A, Salmelin R Dynamic imaging of coherent sources: Studying neuronal interactions in the human brain. PNAS 2001; 98: 694-699

Gross J, Pollok B, Dirks M, Timmermann L, Butz M, Schnitzler A. Task-dependent oscillations during unimanual and bimanual movements in the human primary motor cortex and SMA studied with magnetoencephalography. NeuroImage 2005; 26(1), 91– 98.doi.org/10.1016/j.neuroimage.2005.01.025

Moeller F, Maneshi M, Pittau F, Gholipour T, Bellec P, Dubeau F, Grova C, Gotman J. Functional connectivity in patients with idiopathic generalized epilepsy. Epilepsia 2011;52(3):515-22. doi: 10.1111/j.1528-1167.2010.02938.x.

Hamandi K, Salek-Haddadi A, Laufs H. EEG-fMRI of idiopathic and secondarily generalized epilepsies. NeuroImage 2006;31:1700–1710

Hohl SS, Chaisanguanthum KS, Lisberger SG. Sensory population decoding for visually guided movements. Neuron 2013;79(1):167-79. doi: 10.1016/j.neuron.2013.05.026.

Holmes MD, Quiring J, Tucker DM. Evidence that juvenile myoclonic epilepsy is a disorder of frontotemporal corticothalamic networks. Neuroimage 2010; 49(1):80-93. doi: 10.1016/j.neuroimage.2009.08.004.

Holmes M. D, Brown M, Tucker D. M. Are “Generalized” Seizures Truly Generalized? Evidence of Localized Mesial Frontal and Frontopolar Discharges in Absence. Epilepsia 2004; 45(12), 1568–1579. doi.org/10.1111/j.0013-9580.2004.23204.x.

Duncan JS, Panayiotopoulos CP. Typical absences with specific modes of precipitation (reflex absences): Clinical aspects. In: Duncan JS, Panayiotopoulos CP, editors. Typical absences and related epileptic syndromes. London: Churchill Communications Europe 1995; 206–12.

Jacobs J, Kobayashi E, Boor R, Muhle H, Stephan W, Hawco C, Dubeau F, Jansen O, Stephani U, Gotman J, Siniatchkin M. Haemodynamic responses to interictal epileptiform discharges in children with symptomatic epilepsy. Epilepsia 2007; 48: 2068– 2078.

Jamadar SD, Fielding J, Egan GF. Quantitative meta-analysis of fMRI and PET studies reveals consistent activation in fronto-striatal-parietal regions and cerebellum during antisaccades and prosaccades. Front Psychol 2013; 16;4:749. doi: 10.3389/fpsyg.2013.00749.

Japaridze N, MuthuramanM, Moeller F, Boor R, Anwar AR, Deuschl G, Stephani U, Raethjen J, Siniatchkin M. Neuronal Networks in West Syndrome as Revealed by Source Analysis and Renormalized Partial Directed Coherence. Brain Topogr 2013; 26(1):157-70.

Japaridze N, Siniatchkin M, Muthuraman M, Raethjen J, Stephani U, Moeller F . Dynamic imaging of coherent sources. Identification of neuronal network underlying frequency-associated EEG patterns. Z Epileptol 2013; 26:19-24

Jeavons PM. Nosological problems of myoclonic epilepsies in childhood and adolescence. Dev Med Child Neurol 1977;19(1):3-8. doi: 10.1111/j.1469- 8749.1977.tb08014.x.

Joo MS, Park DS, Moon CT, Chun YI, Song SW, Roh HG. Relationship between gyrus rectus resection and cognitive impairment after surgery for ruptured anterior communicating artery aneurysms. J Cerebrovasc Endovasc Neurosurg 2016;18(3):223- 228.

doi: 10.7461/jcen.2016.18.3.223.

Kane N, Acharya J, Beniczky S. A revised glossary of terms most commonly used by clinical electroencephalographers and updated proposal for the report format of the EEG findings. Clin Neurophysiol Pract 2019; 15;4:133. doi:10.1016/j.cnp.2017.07.002.

Kim DS, Nordli DR, Zelko F. Spectral power of 1–4 Hz frequency in the ictal phase of childhood absence epilepsy. Clin Neurophysiol 2011; 28(5), 1. doi.org/10.1097/WNP.0b013e318231c2e1

Koenig T. Basic Principles of EEG and MEG Analysis, 2014; 1–12.

Kropotov J D. Quantitative EEG, Event-Related Potentials and Neurotherapy. Elsevier Inc 2009; 116-159 doi.org/10.1016/B978-0-12-374512-5.X0001-1.

Labate A, Briellmann RS, Abbott DF, Waites AB, Jackson GD. Typical childhood absence seizures are associated with thalamic activation. Epileptic Disord 2005; 7: 373– 377

Laufs H, Lengler U, Hamandi K, Kleinschmidt A, Krakow K. Linking generalized spike-and-wave discharges and resting state brain activity by using EEG/fMRI in a patient with absence seizures. Epilepsia 2006; 47: 444– 448

Li Q, Chen Y, Wei Y, Chen S, Ma L, He Z, Chen Z. Functional network connectivity patterns between idiopathic generalized epilepsy with myoclonic and absence seizures. Front Comput Neurosci 2017; 11:38. doi: 10.3389/fncom.2017.00038.

Li Q, Luo C, Yang T, Yao Z, He L, Liu L, Xu H, Gong Q, Yao D, Zhou D. EEG-fMRI study on the interictal and ictal generalized spike-wave discharges in patients with childhood absence epilepsy. Epilepsy Res. 2009; 87(2-3):160-8. doi: 10.1016/j.eplepsyres.2009.08.018.

Liu Y, Yang T, Liao W, Yang X, Liu I, Yan B, Chen H, Gong Q, Stefan H, Zhou D. EEG-fMRI study of the ictal and interictal epileptic activity in patients with eyelid myoclonia with absences. Epilepsia 2008; 49(12):2078-86. doi: 10.1111/j.1528-1167.2008.01724.x.

Liu Y, Bengson J, Huang H, Mangun GR, Ding M. Top-down Modulation of Neural Activity in Anticipatory Visual Attention: Control Mechanisms Revealed by Simultaneous EEG-fMRI. Cereb Cortex 2016; 26(2):517-29. doi: 10.1093/cercor/bhu204.

Manganotti P, Tamburin S, Bongiovanni LG, Zanette G, Fiaschi A. Motor responses to afferent stimulation in juvenile myoclonic epilepsy. Epilepsia. 2004; 45(1):77-80. doi: 10.1111/j.0013-9580.2004.21003.x.

Marini C, Romoli M, Parrini E, et al. Clinical features and outcome of 6 new patients carrying de novo KCNB1 gene mutations. Neurol Genet 2017; 3(6):e206.

Meenakshi, D R, Singh A K, Singh A K. Frequency analysis of healthy & epileptic seizure in EEG using fast Fourier transform. Int j eng 2014; 2(4), 683-691.

Michel CM, Murray MM, Lantz G, Gonzalez S, Spinelli L, Grave de Peralta R. EEG source imaging. Clin Neurophysiol 2004; 115(10):2195-222. doi: 10.1016/j.clinph.2004.06.001.

Michel CM, Murray MM. Towards the utilization of EEG as a brain imaging tool. Neuroimage 2012; 61(2):371-85. doi: 10.1016/j.neuroimage.2011.12.039.

Michel C, Koenig T, Brandeis D, Gianotti L, Wackermann J. Electrical Neuroimaging. In Scalp field maps and their characterization. Cambridge: Cambridge University Press 2009; 25-48. doi:10.1017/CBO9780511596889

Moeller F, Muthuraman M, Stephani U, Deuschl G, Raethjen J, Siniatchkin M. Representation and Propagation of Epileptic Activity in Absences and Generalized Photoparoxysmal Responses. Human Brain Mapping 2013; 34(8): 1896-909

Moeller F, Siebner H, Ahlgrimm N, Wolff S, Muhle H, Granert O, Boor R, Jansen O, Gotman J, Stephani U, Siniatchkin M. fMRI activation during spike and wave discharges evoked by photic stimulation. NeuroImage 2009; 48. 682-95.

Morecraft RJ, Louie J L, Herrick JL, Stilwell-Morecraft KS. Cortical innervation of the facial nucleus in the non-human primate: a new interpretation of the effects of stroke and related subtotal brain trauma on the muscles of facial expression. Brain, 2001; 124(1), 176-208.

Mourente-Diaz S, Montenegro MA, Lowe JP, Akman CI. Unusual focal ictal pattern in children with eyelid myoclonia and absences. Pediatr Neurol 2007; 37:292-295.

Moutaouakil F, El Otmani H, Fadel H, El Moutawakkil B, Slassi I. Benign myoclonic epilepsy of infancy evolving to Jeavons syndrome. Pediatr Neurol 2010; 43(3):213-6.

Nolte G, Bai O, Wheaton L, Mari Z, Vorbach S, Hallett M. Identifying true brain interaction from EEG data using the imaginary part of coherency. Clinical Neurophysiology 2004; 115(10), 2292–2307.

Nunez P L, Srinivasan R, Westdorp A F, Wijesinghe R S, Tucker D M, Silberstein R B, Cadusch P J. EEG coherency I: Statistics, reference electrode, volume conduction, Laplacians, cortical imaging, and interpretation at multiple scales. Electroencephalogr and Clin Neurophysiol 1997; 103(5), 499–515. doi.org/10.1016/S0013-4694(97)00066- 7

Oguni H, Mukahira K, Oguni M, Uehara T, Su YH, Izumi T, Fukuyama Y. Video-polygraphic analysis of myoclonic seizures in juvenile myoclonic epilepsy. Epilepsia 1994; 35(2):307-16. doi: 10.1111/j.1528-1157.1994.tb02435.x.

Ogura K, Maegaki Y, Koeda T. EEG evaluation of Fixation-off sensitivity in eyelid Myoclonia with absences. Pediatr Neurol 2005; 33 142-14.

Ohya T, Yamashita Y, Shibuya I, Hara M, Nagamitsu S, Matsuishi T. Eyelid myoclonia with absences occurring during the clinical course of cryptogenic myoclonic epilepsy of early childhood. Eur J Pediatr Neurl 2012; 16 (4): 399-401.

O'Muircheartaigh J, Richardson MP. Epilepsy and the frontal lobes. Cortex 2012; 48(2):144-55. doi: 10.1016/j.cortex.2011.11.012.

O'Muircheartaigh J, Vollmar C, Barker G J, Kumari , Symms M R, Thompson P, Duncan J S, Koepp M J, Richardson M P. Focal structural changes and cognitive dysfunction in juvenile myoclonic epilepsy. Neurology 2011; 76(1), 34–40. doi.org/10.1212/WNL.0b013e318203e93d

Oostenveld R, Stegeman D F, Praamstra P, Van Oosterom A. Brain symmetry and topographic analysis of lateralized event-related potentials. Clin Neurophysiol 2003; 114(7), 1194–1202. doi.org/10.1016/S1388-2457(03)00059-2

Panayiotopoulos C P, Jeavons syndrome. In: Panayiotopoulos CP, editor. The epilepsies: Seizures, Syndromes and Management, 2005: 475-80.

Panayiotopoulos CP. Reflex seizures and related epileptic syndromes. In: Panayiotopoulos CP, editor. A clinical Guide to Epileptic Syndromes and Their treatment, 2010: 514-515.

Panzica F, Rubboli G, Franceschetti S, Avanzini G, Meletti S, Pozzi A, Tassinari CA. Cortical myoclonus in Janz syndrome. Clin Neurophysiol 2001; 112(10):1803-9. doi: 10.1016/s1388-2457(01)00634-4.

Parker A, Gardiner R M, Panayiotopoulos CP, Agathonikou A, Ferrie C. Observations on families of patients with eyelid myoclonia with absences. In Duncan JS, Panayiotopoulos CP. Eyelid Myoclonia with absences. London: John Libbey and Company LTD, 1996; 107-14.

Pascual-Marqui RD, Lehmann D, Koukkou M, Kochi K, Anderer P, Saletu B, Tanaka H, Hirata K, John ER, Prichep L, Biscay-Lirio R, Kinoshita T. Assessing interactions in the brain with exact low-resolution electromagnetic tomography. Philos Trans A Math Phys Eng Sci 2011; 13;369(1952):3768-84. doi: 10.1098/rsta.2011.0081.

Pascual-Marqui R D. Standardized low resolution brain electromagnetic tomography (sLORETA): technical details. Methods Find Exp Clin Pharmacol 2002; 24D:5-12. 5– 12.

Pascual-Marqui R D, Michel C M, Lehmann D. Low resolution electromagnetic tomography: a new method for localizing electrical activity in the brain. Int J Psychophysiol 1994; 18(1), 49–65. doi.org/10.1016/0167-8760(84)90014-X

Pascual-Marqui R D. Discrete, 3D distributed, linear imaging methods of electric neuronal activity. Part 1: exact, zero error localization 2007; http://arxiv.org/abs/0710.3341

Pierrot-Deseilligny C, Milea D, Müri RM. Eye movement control by the cerebral cortex. Curr Opin Neurol 2004; 17(1):17-25. doi: 10.1097/00019052-200402000-00005.

Pugnaghi M, Carmichael DW, Vaudano AE, Chaudhary UJ, Benuzzi F, Di Bonaventura C, Giallonardo AT, Rodionov R, Walker MC, Duncan JS, Meletti S, Lemieux L. Generalized spike and waves: effect of discharge duration on brain networks as revealed by BOLD fMRI. Brain Topogr 2014;27(1):123-37. doi: 10.1007/s10548-013-0311-0.

Purushothaman G, Marion R, Li K, Casagrande VA. Gating and control of primary visual cortex by pulvinar. Nat Neurosci 2012;15(6):905-12. doi: 10.1038/nn.3106.

Qin Y, Jiang S, Zhang Q, Dong L, Jia X, He H, Yao Y, Yang H, Zhang T, Luo C, Yao

D. BOLD-fMRI activity informed by network variation of scalp EEG in juvenile myoclonic epilepsy. Neuroimage Clin 2019; 22:101759. doi: 10.1016/j.nicl.2019.101759.

Radovici MM, Misirliou VL, Gluckman M. Epilepsie reflexe provoquee par excitations optiques des rayons solaires. Revue Neurologique 1932;1:1305-8.

Raichle ME, MacLeod AM, Snyder AZ, Powers WJ, Gusnard DA, Shulman GL. A default mode of brain function. Proc Natl Acad Sci U S A 2001; 98(2):676-82. doi: 10.1073/pnas.98.2.676.

Routley B, Shaw A, Muthukumaraswamy SD, Singh KD, Hamandi K. Juvenile myoclonic epilepsy shows increased posterior theta, and reduced sensorimotor beta resting connectivity. Epilepsy Res 2020;163:106324. doi: 10.1016/j.eplepsyres.2020.106324.

Rudolf G, Lesca G, Mehrjouy MM, Labalme A, Salmi M, Bache I, Bruneau N, Pendziwiat M, Fluss J, de Bellescize J, Scholly J, Møller RS, Craiu D, Tommerup N, Valenti-Hirsch MP, Schluth-Bolard C, Sloan-Béna F, Helbig KL, Weckhuysen S, Edery P, Coulbaut S, Abbas M, Scheffer IE, Tang S, Myers CT, Stamberger H, Carvill GL, Shinde DN, Mefford HC, Neagu E, Huether R, Lu HM, Dica A, Cohen JS, Iliescu C, Pomeran C, Rubenstein J, Helbig I, Sanlaville D, Hirsch E, Szepetowski P. Loss of function of the retinoid-related nuclear receptor (RORB) gene and epilepsy. Eur J Hum Genet 2016; 24(12):1761-1770. doi: 10.1038/ejhg.2016.80.

Rubboli G, Meletti S, Gardella E, Zaniboni A, d'Orsi G, Dravet C, Tassinari CA. Photic reflex myoclonus: a neurophysiological study in progressive myoclonus epilepsies. Epilepsia 1999; 40 Suppl 4:50-8. doi: 10.1111/j.1528-1157.1999.tb00907.x.

Ruff DA, Cohen MR. Pursuing the link between neurons and behavior. Neuron 2013; 79(1):6-9. doi: 10.1016/j.neuron.2013.06.045.

Sadleir L G, Vears D, Regan B, Redshaw N, Bleasel A, Scheffer I E Family studies of individuals with eyelid Myoclonia. Epilepsia 2012; 53(12):2141-2148.

Salek-Haddadi A, Lemieux L, Merschhemke M, Friston KJ, Duncan JS, Fish DR. Functional magnetic resonance imaging of human absence seizures. Ann Neurol 2003; 53: 663–667

Salman A, Turovets S, Malony, A., Eriksen, J., & Tucker, D. Computational modeling of human head conductivity. Lecture Notes in Computer Science 2005; 3514(I), 631–638. https://doi.org/10.1007/11428831_78

Samanta D, Willis E. KIAA2022-related disorders can cause Jeavons (eyelid myoclonia with absence) syndrome. Acta Neurol Belg 2020;120(1):205-207. doi: 10.1007/s13760-018-0887-y.

Schelter B, Timmer J, Eichler M. 2009. Assessing the strength of directes influences among neural signals using renormalized partial directed coherence. J Neurosci Methods 2009; 179, 121-30

Sevgi EB, Saygi S, Ciger A. Eye closure sensitivity and epileptic syndromes: A retrospective study of 26 adult cases. Seizure 2007;16(1):17-21. doi: 10.1016/j.seizure.2006.09.004.

Shim M, Hwang HJ, Kim DW, Lee SH, Im CH. Machine-learning-based diagnosis of schizophrenia using combined sensor-level and source-level EEG features. Schizophr Res 2016; 176(2-3):314-319. doi: 10.1016/j.schres.2016.05.007.

Siniatchkin M, Groening K, Moehring J, Moeller F, Boor R, Brodbeck V, Michel C M, Rodionov R, Lemieux L, Stephani U. Neuronal network in children with continuous spikes and waves during slow sleep. Brain 2010; 133(9), 2798-813.

Siniatchkin M, Groppa S, Jerosch B, Muhle H, Kurth C, Shepherd AJ, Siebner H, Stephani U. Spreading photoparoxysmal EEG response is associated with an abnormal cortical excitability pattern. Brain 2007;130(Pt 1):78-87. doi: 10.1093/brain/awl306.

Song J, Tucker DM, Gilbert T, Hou J, Mattson C, Luu P, et al. Methods for examining electrophysiological coherence in epileptic networks. Front Neurol 2013;4:55.

Stefan H, Paulini-Ruf A, Hopfengärtner R, Rampp S. Network characteristics of idiopathic generalized epilepsies in combined MEG/EEG. Epilepsy Res 2009; 85(2- 3):187-98. doi: 10.1016/j.eplepsyres.2009.03.015.

Striano S, Capovilla G, Sofia V, Romeo A, Rubboli G, Striano P, Trenité DK. Eyelid myoclonia with absences (Jeavons syndrome): a well-defined idiopathic generalized epilepsy syndrome or a spectrum of photosensitive conditions? Epilepsia. 2009; 50, 5:15-9. doi: 10.1111/j.1528-1167.2009.02114.x.

Suckling J, Bullmore E. Permutation tests for factorially designed neuroimaging experiments. Hum Brain Mapp 2004; 22(3), 193–205. doi.org/10.1002/hbm.20027

Thieu T, Yang H. Diagnosis of Epilepsy in Patients Based on the Classification of EEG Signals Using Fast Fourier Transform. In Proceedings of the 28th International Conference on Current Approaches in Applied Artificial Intelligence 2015; 9101. 493- 500.

Tharp BR, Gersch W. Spectral analysis of seizures in humans. Comput Biomed Res 1975;8(6):503-21. doi: 10.1016/0010-4809(75)90023-3.

Tzourio-Mazoyer N, Landeau B, Papathanassiou D, Crivello F, Etard O, Delcroix N, Mazoyer B, Joliot M. Automated anatomical labeling of activations in SPM using a macroscopic anatomical parcellation of the MNI MRI single-subject brain. NeuroImage 2002; 15(1), 273–289. doi.org/10.1006/nimg.2001.0978

Vaudano AE, Ruggieri A, Tondelli M, Avanzini P, Benuzzi F, Gessaroli G, Cantalupo G, Mastrangelo M, Vignoli A, Bonaventura CD, Canevini MP, Bernardina BD, Nichelli PF, Meletti S. The visual system in eyelid myoclonia with absences. Ann Neurol 2014; 76(3):412-27. doi: 10.1002/ana.24236.

Vaudano A E, Laufs H, Kiebel S J, Carmichael D W, Hamandi K, Guye M, Thornton R, Rodionov R, Friston K J, Duncan J S, Lemieux L. Causal hierarchy within the thalamo-cortical network in spike and wave discharges. PloS one 2009; 4(8), e6475. doi.org/10.1371/journal.pone.0006475

Viravan S, Go C, Ochi A, Akiyana T, Otsubo H. Jeavons syndrome existing as occipital cortex initiating generalized epilepsy. Epilepsia 2011; 52(7):1273-9.

Vulliemoz S, Vollmar C, Koepp MJ, Yogarajah M, O'Muircheartaigh J, Carmichael DW, Stretton J, Richardson MP, Symms MR, Duncan JS. Connectivity of the supplementary motor area in juvenile myoclonic epilepsy and frontal lobe epilepsy. Epilepsia 2011; 52(3):507-14. doi: 10.1111/j.1528-1167.2010.02770.

Waltz S, Christen HJ, Doose H. The different patterns of the photoparoxysmal response: a genetic study. Electroencephalogr Clin Neurophysiol 1992; 83(2):138-45. doi: 10.1016/0013-4694(92)90027-f.

Wilkins AJ, Baker A, Amin D. Treatment of photosensitive epilepsy using coloured glasses. Seizure 1999; 8(8):444-9.

Wilkins AJ, Bonanni P, Porciatti V, Guerrini R. Physiology of human photosensitivity. Epilepsia 2004; 45, 1:7-13. doi: 10.1111/j.0013-9580.2004.451009.x.

Zhang Z. A fast method to compute surface-potentials generated by dipoles within multilayer aniosotropic spheres. Phys Med Biol, 1995; 40, 335-349.

Zhong C, Liu R, Luo C, Jiang S, Dong L, Peng R, Guo F, Wang P. Altered Structural and Functional Connectivity of Juvenile Myoclonic Epilepsy: An fMRI Study. Neural plasticity 2018; 7392187. doi.org/10.1155/2018/7392187

Zou Q, Long X, Zuo X, Yan C, Zhu C, Yang Y, Liu D, He Y, Zang Y. Functional connectivity between the thalamus and visual cortex under eyes closed and eyes open conditions: a resting-state fMRI study. Hum Brain Mapp 2009; 30(9):3066-78. doi: 1002/hbm.20728

8. Supplementary material

8.1.Source results for non-normalised data

Applying two-way repeated measure ANOVA showed a significant effect only of time for all frequency bands. There was no significant effect found for group and interaction effect.

a) Delta band

For the delta band two-way repeated measure ANOVA showed no significant group effect or interaction effect. It showed a significant time effect with the source of the strongest power in the right and left occipital region (in the right and left cuneus gyrus), mni coordinates [4.0 -86.0 20.0] mm. Post hoc test for time effect revealed that during ictal/interictal segments had a stronger source power compared to pre-ictal/interictal segments. The significant difference with a maximum of power between during ictal/interictal intervals and pre- ictal/interictal intervals was localised in left frontal rectus gyrus; (mni coordinates [-2.0 12.0 -26.0] mm) (Figure 18).

b) Theta band

For theta band two-way repeated ANOVA showed the strongest power without labelled, with mni coordinates [4.0 -100.0 28.0] mm. After applying post hoc test the significant source maximum was localised in the left frontal rectus gyrus (mni coordinates [-2.0 20.0 -26.0] mm) (Figure 19).

c) Alpha band

The ANOVA result for alpha band showed the strongest power in the right occipital region, in the right calcarine gyrus (mni coordinates [20.0 -104.0 -2.0] mm). After performing the post hoc test for time effect the source of maximal power showed no label (NA) (mni coordinates [-2.0 20.0 -32.0] mm). The nearest strongest label was in the right and left frontal rectus gyrus (mni coordinates [2.0 16.0 -24.0] mm) (Figure 20).

d) Beta band

After applying two-way repeated ANOVA for the beta band the strongest power was not labelled (mni coordinates [4.0 -86.0 -48.0] mm). After the post hoc test the strongest source power was again without label (NA) (mni coordinates [2.0 28.0 -32.0] mm) but the nearest strongest label was in the right frontal rectus gyrus (mni coordinates [2.0 32.0 -24.0] mm) (Figure 21).

Figure 18. Source results for the delta frequency band

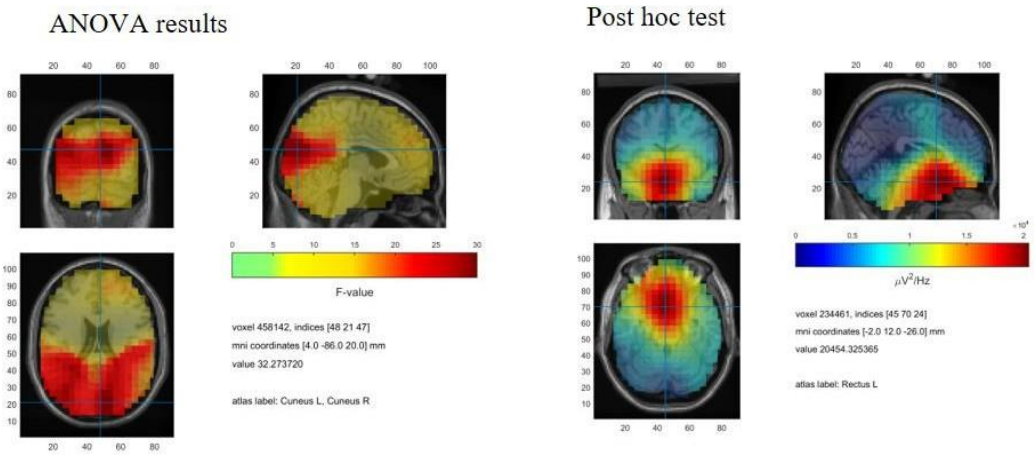

Figure 19. Source results for the theta frequency band

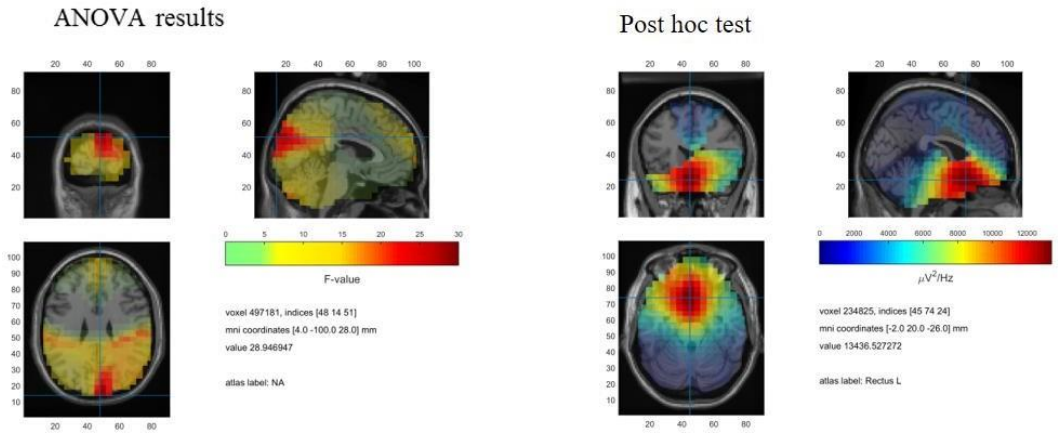

Figure 20. Source results for the alpha frequency band

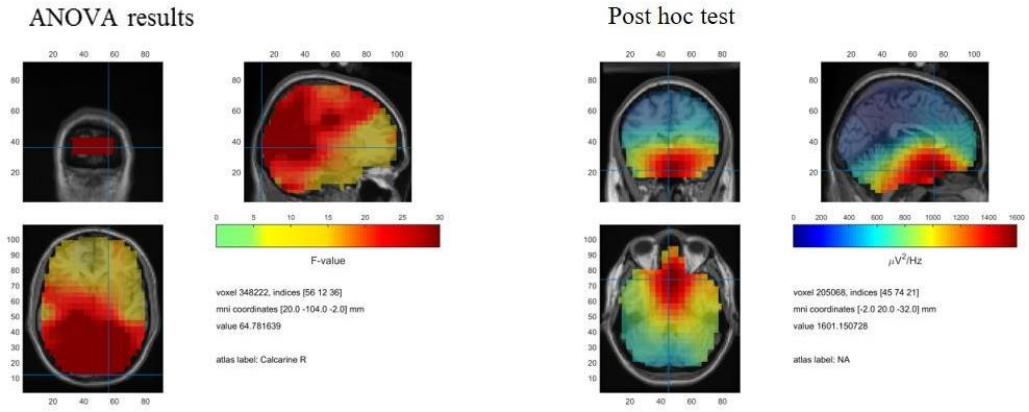

Figure 21. Source results for the beta frequency band

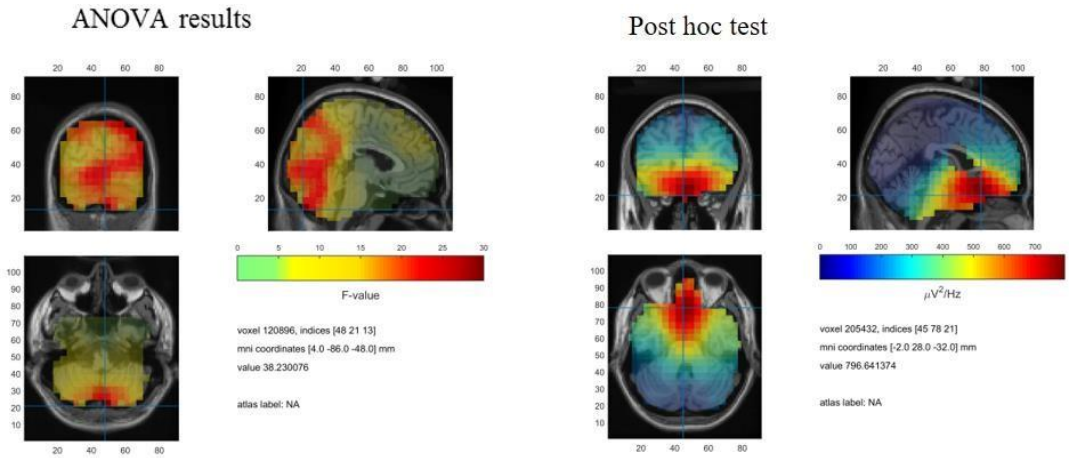

8.2 The imaginary part of coherency using source maximum as a seed for non-normalised data

Comparing the imaginary part of coherency for all four-frequency bands after ANOVA test the significant main effect only of time was detected. For group and interaction effect there was no significant difference detected in any bands.

Post-hoc test for the main effect of time showed that during ictal/ during interictal interval has higher iCoh compare with pre-ictal/pre-interictal in all four frequency bands.

1. For the delta band, the strongest coherence with the source maximum (left rectus gyrus) was detected in the right parietal region, right supramarginal gyrus (mni coordinates [42.0 -32.0 28.0] mm) (Figure 22).

2. At the theta frequency band, the strongest coherent region for the source maximum (left rectus gyrus) was without a label (NA) (mni coordinates [-32.0 -48.0 28.0] mm). The closet strongest label was localised in the left parietal region, left parietal inferior gyrus (mni coordinates [-38.0 -38.0 36.0] mm) (Figure 23).
3. For the alpha band the strongest coherence with the reference source (NA/right and left frontal rectus gyrus) was detected in the right occipital region, right occipital superior gyrus and right occipital middle gyrus (mni coordinates [28.0 -62.0 34.0] mm) (Figure 24).

4. For the beta band, the strongest coherence with the reference source (NA/right frontal rectus gyrus) was detected in the right parietal region, right angular Gyrus (mni coordinates [42.0 -78.0 42.0] mm) (Figure 25).

Figure 22. The imaginary part of coherency for the delta frequency band

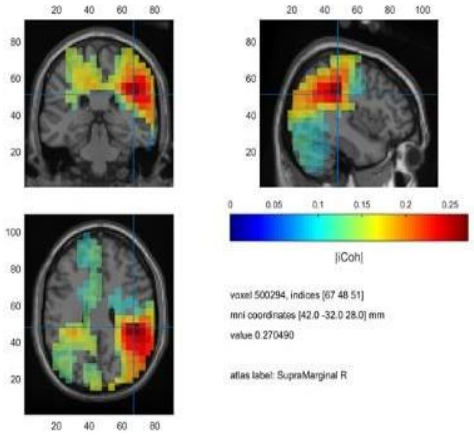

Figure 23. The imaginary part of coherency for the theta frequency band

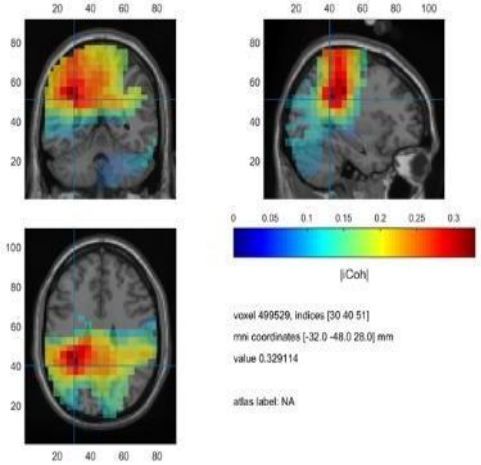

Figure 24. The imaginary part of coherency for the alpha frequency band

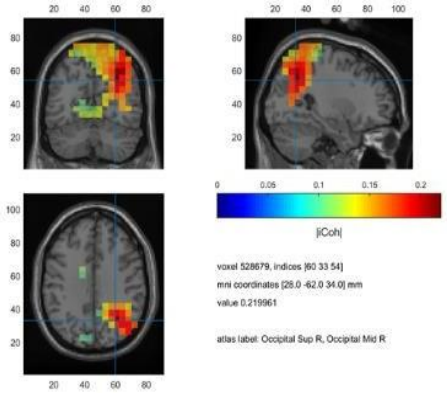

Figure 25. The imaginary part of coherency for the beta frequency band

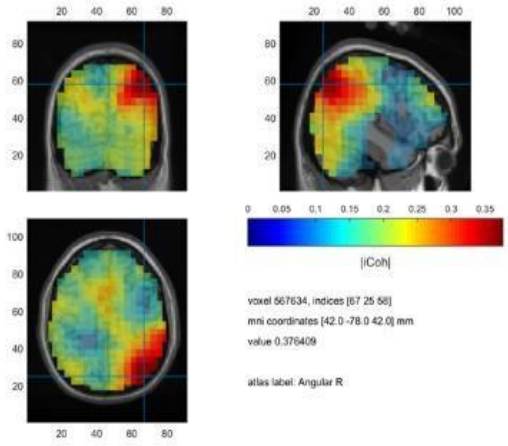

8.3 The imaginary part of coherency using thalamus as a seed for non-normalizes data

Comparing the imaginary part of coherency for all four frequency bands after ANOVA test the significant main effect only of time was detected. For group and interaction effect there was no significant difference detected in any bands.

Post-hoc test for the main effect of time showed that during ictal/ during interictal interval has higher iCoh compare with pre-ictal/pre-interictal in three (delta, theta, beta) frequency bands.

1. For the delta band, the strongest coherence with the thalamus was not labelled (mni coordinates [42.0 -40.0 28.0] mm) and the nearest strongest label was detected in the right parietal region, right supramarginal gyrus (mni coordinates [44.0 -40.0 34.0] mm) (Figure 26).

2. At the theta frequency band, the strongest coherent region for the thalamus was localised in the left parietal region, left parietal superior gyrus (mni coordinates [-32.0 -48.0 72.0] mm) (Figure 27).
3. For the alpha band, the strongest connection with the thalamus was detected in the right parietal region, in the right postcentral gyrus and right precuneus gyrus (mni coordinates [12.0 -48.0 72.0] mm) (Figure 28).
4. For the beta band, the strongest connection with the thalamus was detected in the right parietal region, in the right angular gyrus (mni coordinates [50.0 -70.0 42.0] mm) (Figure 29).

Figure 26 . Imaginary part of coherency using thalamus as a seed for delta band

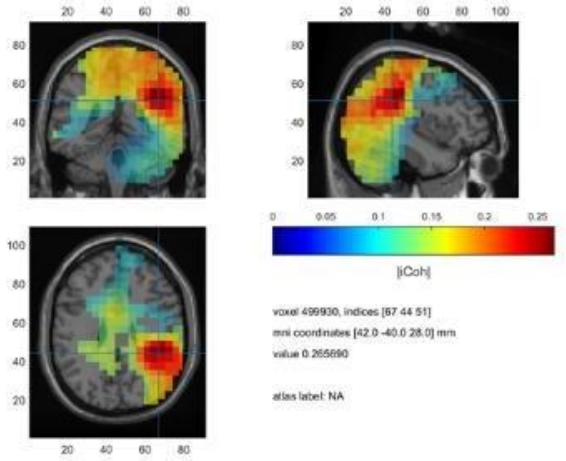

Figure 27. Imaginary part of coherency using thalamus as a seed for the theta band

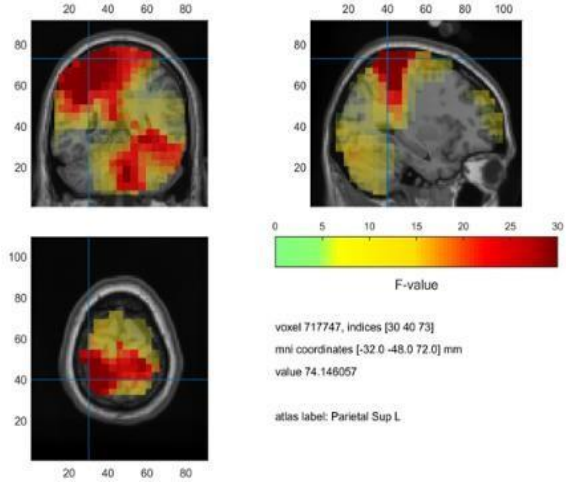

Figure 28. Imaginary part of coherency using thalamus as a seed for the alpha band

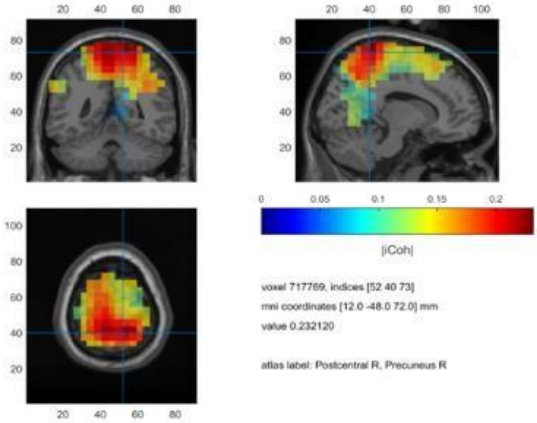

Figure 29. Imaginary part of coherency using thalamus as a seed for the beta band

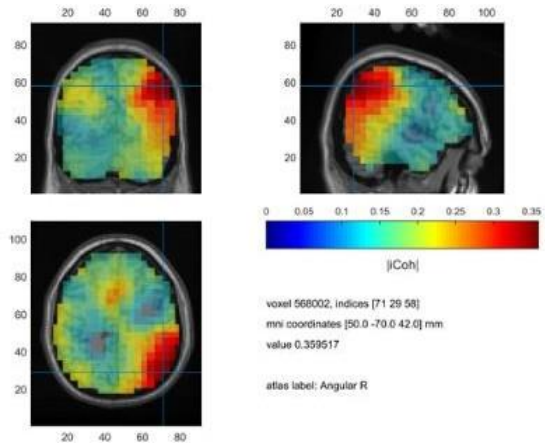

8.4 The imaginary part of coherency using source analysis results receivedafter ANOVA test as a seed for normalizes data

Comparing the imaginary part of coherency for all four frequency bands after ANOVA test thesignificant main effect only of time was detected (except for alpha band). For group and interaction effect there was no significant difference detected in any bands.

Post-hoc test for the main effect of time showed that during ictal/ during interictal interval hashigher iCoh compare with pre-ictal/pre-interictal in three (delta, theta, beta) frequency bands.

Figure 30. iCoh for delta band using right calcarin as a seed

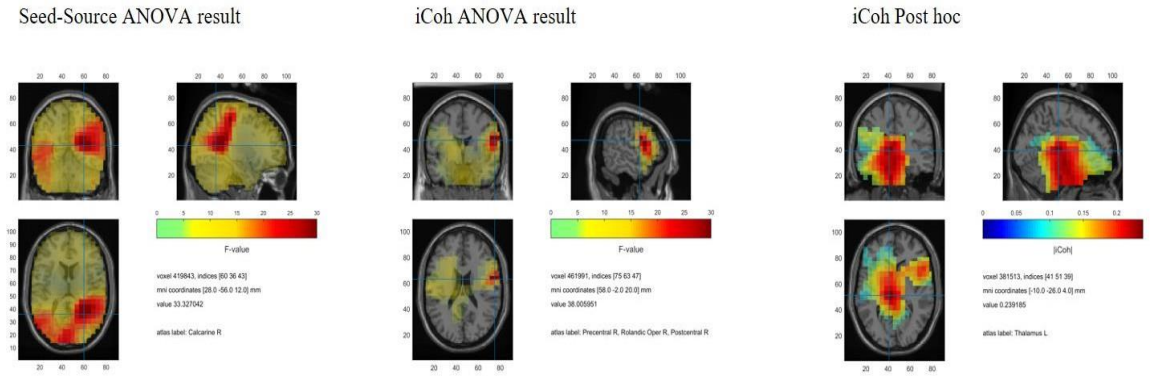

Figure 31. iCoh for theta band using right parietal inferior and right supramarginal gyrus as aseed

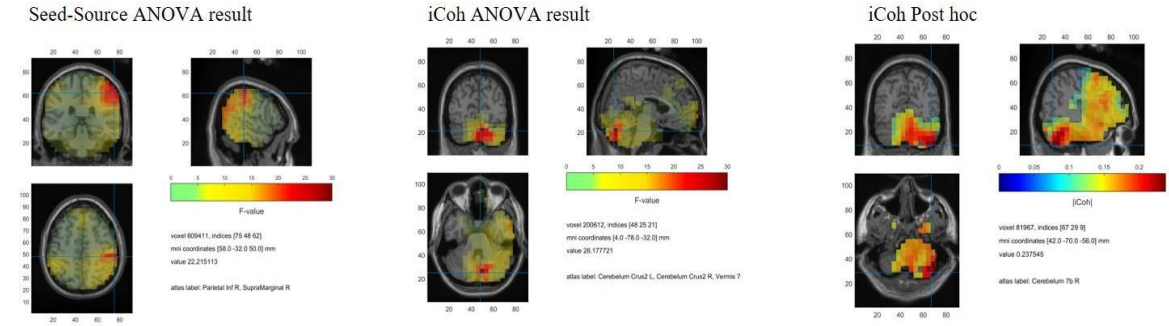

Figure 32. iCoh for alpha band using right Cuneus as a seed

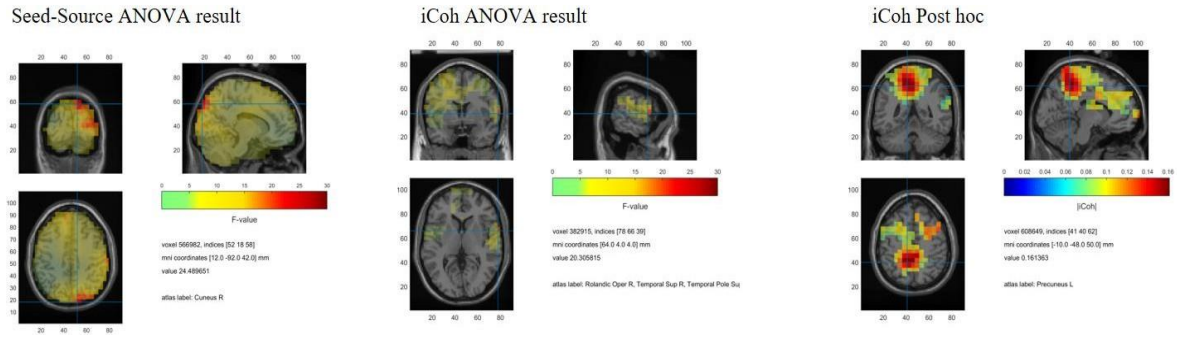

Figure 33. iCoh for beta band using the right superior parietal gyrus as a seed

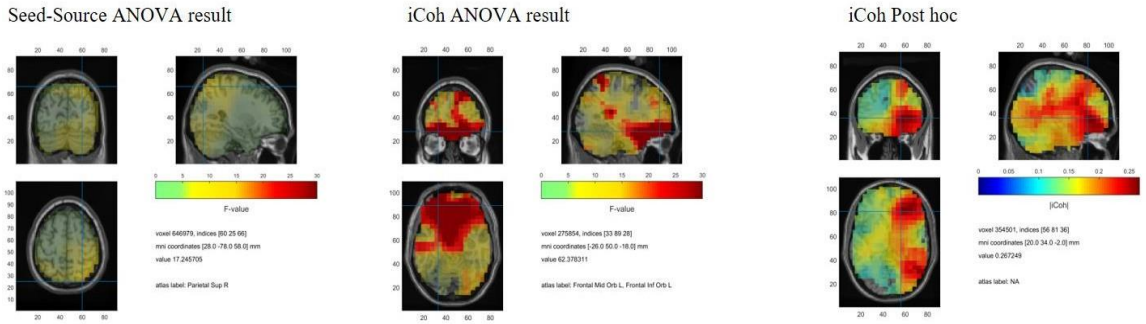

8.5 The imaginary part of coherency using source analysis results receivedafter ANOVA test as a seed for non-normalizes data

Comparing the imaginary part of coherency for all four frequency bands after ANOVA test thesignificant main effect only of time was detected for three bands: Alpha, theta and beta frequency bands. For group and interaction effect there was no significant difference detectedin these three bands. Post-hoc test for the main effect of time showed that during ictal/ during interictal interval has higher iCoh compare with pre-ictal/pre-interictal in three (alpha, theta, beta) frequency bands.

Only the delta bend was exceptional, which showed a significant effect of group (ictal/interictal)after ANOVA test. Post-hoc test for the effect of group showed that ictal interval has higher iCoh compare with interictal interval for the delta frequency bands.

Figure 34. iCoh for delta band using the left and right cuneus as a seed

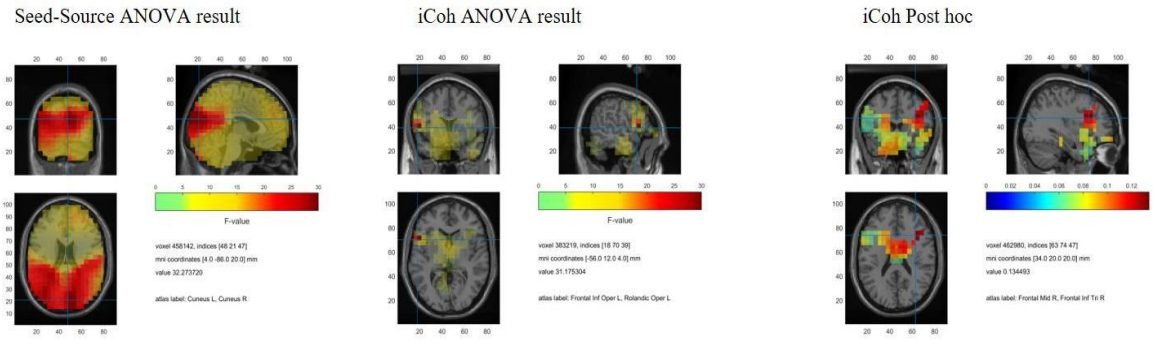

Figure 35. iCoh for theta band using NA gyrus as a seed

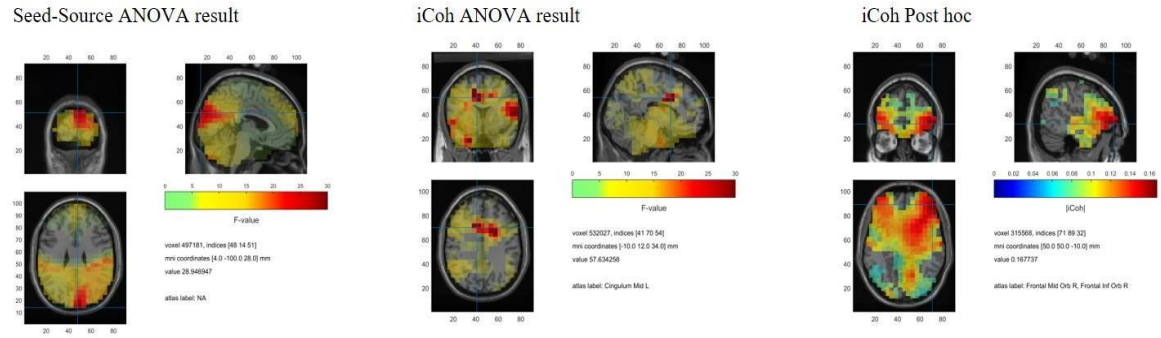

Figure 36. iCoh for alpha band using right calcarin gyrus as a seed

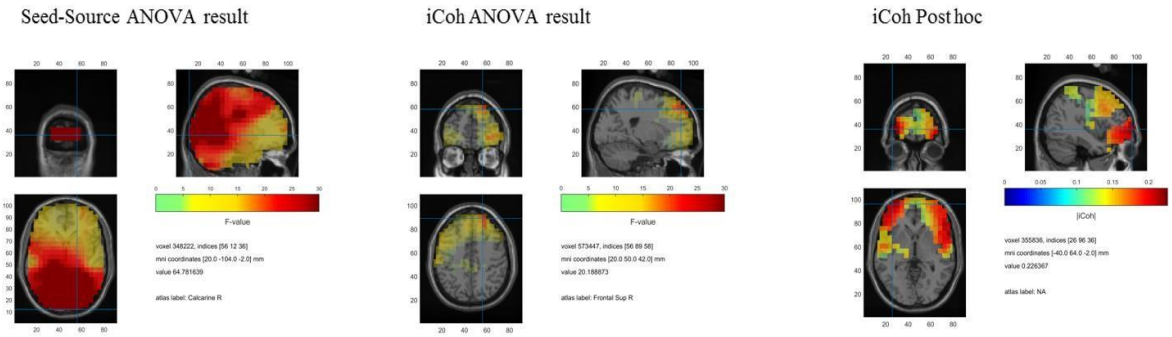

Figure 37. iCoh for delta band using NA gyrus as a seed